Circulation Research

ORIGINAL RESEARCH

An ERK5-NRF2 Axis Mediates Senescence-Associated Stemness and Atherosclerosis

Jun-ichi Abe,* Masaki Imanishi,* Shengyu Li,* Aijun Zhang, Kyung Ae Ko, Venkata S.K. Samanthapudi, Ling-Ling Lee, Angelica Paniagua Bojorges, Young Jin Gi, Brian P. Hobbs, Anita Deswal, Joerg Herrmann, Steven H. Lin, Eduardo N. Chini, Ying H. Shen, Keri L. Schadler, Thi-Hong-Minh Nguyen, Anisha A. Gupte, Cielito Reyes-Gibby, Sai-Ching J. Yeung, Rei J. Abe, Elizabeth A. Olmsted-Davis, Sunil Krishnan, Robert Dantzer, Nicolas L. Palaskas, John P. Cooke, Henry J. Pownall, Momoko Yoshimoto, Keigi Fujiwara, Dale J. Hamilton,† Jared K. Burks,† Guangyu Wang,‡ Nhat-Tu Le,‡ Sivareddy Kotla‡

BACKGROUND: ERK5 (extracellular signal-regulated kinase 5) is a dual kinase transcription factor containing an N-terminal kinase domain and a C-terminal transcriptional activation domain. Many ERK5 kinase inhibitors have been developed and tested to treat cancer and inflammatory diseases. However, recent data have raised questions about the role of the catalytic activity of ERK5 in proliferation and inflammation. We aimed to investigate how ERK5 reprograms myeloid cells to the proinflammatory senescent phenotype, subsequently leading to atherosclerosis.

METHODS: A ERK5 S496A (dephosphorylation mimic) knock in (KI) mouse model was generated using CRISPR/Cas9 (clustered regularly interspaced short palindromic repeats/clustered regularly interspaced short palindromic repeat–associated 9), and atherosclerosis was characterized by hypercholesterolemia induction. The plaque phenotyping in homozygous ERK5 S496A KI and wild type (WT) mice was studied using imaging mass cytometry. Bone marrow–derived macrophages were isolated from hypercholesterolemic mice and characterized using RNA sequencing and functional in vitro approaches, including senescence, mitochondria reactive oxygen species, and inflammation assays, as well as by metabolic extracellular flux analysis.

RESULTS: We show that atherosclerosis was inhibited in ERK5 S496A KI mice. Furthermore, ERK5 S496 phosphorylation mediates both senescence-associated secretory phenotype and senescence-associated stemness by upregulating AHR (aryl hydrocarbon receptor) in plaque and bone marrow–derived macrophages isolated from hypercholesterolemic mice. We also discovered that ERK5 S496 phosphorylation could induce NRF2 (NFE2-related factor 2) SUMOylation at a novel K518 site to inhibit NRF2 transcriptional activity without altering ERK5 catalytic activity and mediates oxidized LDL (low-density lipoprotein)–induced senescence-associated secretory phenotype. Specific ERK5 kinase inhibitors (AX15836 and XMD8-92) also inhibited ERK5 S496 phosphorylation, suggesting the involvement of ERK5 S496 phosphorylation in the anti-inflammatory effects of these ERK5 kinase inhibitors.

CONCLUSIONS: We discovered a novel mechanism by which the macrophage ERK5-NRF2 axis develops a unique senescence-associated secretory phenotype/stemness phenotype by upregulating AHR to engender atherogenesis. The finding of senescence-associated stemness phenotype provides a molecular explanation to resolve the paradox of senescence in proliferative plaque by permitting myeloid cells to escape the senescence-induced cell cycle arrest during atherosclerosis formation.

GRAPHIC ABSTRACT: A graphic abstract is available for this article.

Key Words: antioxidants ■ atherosclerosis ■ mitogen-activated protein kinase 7 (ERK5) ■ NF-E2-related factor 2 (NRF2) ■ receptors, aryl hydrocarbon (AHR) ■ senescence-associated secretory phenotype ■ sumoylation

In This Issue, see p 2 | Meet the First Author, see p 3

Correspondence to: Jun-ichi Abe, MD, PhD, The University of Texas MD Anderson Cancer Center, Houston, TX, Email jabe@mdanderson.org or Sivareddy Kotla, PhD, The University of Texas MD Anderson Cancer Center, Houston, TX, Email skotla@mdanderson.org
*J.-i. Abe, M. Imanishi and S. Li contributed equally.
†D.J. Hamilton and J.K. Burks contributed equally.
‡G. Wang, N.-T. Le, and S. Kotla were equivalent cosenior authors.
Supplemental Material is available at https://www.ahajournals.org/doi/suppl/10.1161/CIRCRESAHA.122.322017.
For Sources of Funding and Disclosures, see page 42.

Circulation Research is available at www.ahajournals.org/journal/res

Novelty and Significance

What Is Known?

- Senescence-associated secretory phenotype is vital in instigating atherosclerosis and tumorigenesis.
- Senescence reprograms cancer cells to acquire a proliferative phenotype (senescence-associated stemness [SAS]) after cancer therapy, which allows them to escape senescence-induced cell cycle arrest.
- ERK5 (extracellular signal-regulated kinase 5) is a dual kinase transcription factor containing an N-terminal kinase domain and a C-terminal transcriptional activation domain, and ERK5 S496 phosphorylation inhibits ERK5 transcriptional activity and subsequently induces senescence-associated secretory phenotype.

What New Information Does This Article Contribute?

- We have identified the SAS phenotype of myeloid cells (MCs) that escaped the growth-suppression effects of p53 (tumor protein p53) in the plaque.
- ERK5 S496 phosphorylation triggered not only senescence-associated secretory phenotype but also SAS by upregulating AHR (aryl hydrocarbon receptor) in MCs and promoting atherosclerosis formation.
- ERK5 S496 phosphorylation induces a novel site (K518) of NRF2 (NFE2-related factor 2) SUMOylation and inhibits NRF2 transcriptional activity without affecting ERK5 catalytic activity.

The involvement of senescence in atherosclerosis formation is now well established; however, cell cycle arrest is the hallmark of senescence, and MC proliferation plays a crucial role in developing atherosclerosis. Therefore, it is challenging to link MC senescence to plaque formation. Using an imaging mass cytometry approach, we discovered the unique MC phenotype of SAS in the plaque, which permits MCs to escape the senescence-induced cell cycle arrest during atherosclerosis formation. This can resolve the paradox of MC senescence observed in proliferative plaque formation. We also demonstrated the crucial role of ERK5 S496 phosphorylation in upregulating MC SAS phenotype in the plaque. RNA sequencing from bone marrow–derived macrophages isolated from normal and hypercholesterolemia mice indicated the possible role of AHR. The depletion of AHR inhibited the increase of senescence-associated β-gal^{+}Ki67^{+} macrophages, supporting the pivotal role of AHR in hypercholesterolemia-induced SAS. ERK5 S496 phosphorylation upregulates NRF2 SUMOylation (K518) and inhibits NRF2 transcriptional activity, which induces AHR in an ERK5 catalytic activity–independent manner. These data indicate a critical role of ERK5 S496 phosphorylation–mediated NRF2 SUMOylation in both senescence-associated secretory phenotype and SAS induction and, consequently, accelerated atherosclerosis. These data provide a novel framework for therapeutic intervention to inhibit atherosclerosis by controlling senescence.

Nonstandard Abbreviations and Acronyms

53BP1	p53-binding protein 1
AHR	aryl hydrocarbon receptor
BMDM	bone marrow–derived macrophage
DNMT3A	DNA methyltransferase 3a
EC	endothelial cell
ERK5	extracellular signal-regulated kinase 5
GAS6	growth arrest-specific protein 6
HFD	high-fat diet
IL	interleukin
IMC	imaging mass cytometry
KI	knock in
KLF2	kruppel-like factor 2
MC	myeloid cell
mtROS	mitochondrial reactive oxygen species
NCD	normal chow diet
NRF2	NFE2-related factor 2
oxLDL	oxidized low-density lipoprotein
p53	tumor protein p53
p90RSK	p90 ribosomal S6 kinase
ROS	reactive oxygen species
SAS	senescence-associated stemness
SASP	senescence-associated secretory phenotype
TEY	threonine-x-tyrosine
TNFα	tumor necrosis factor alpha
TRX1	thioredoxin 1
VSMC	vascular smooth muscle cell
WT	wild type

Age is a significant risk factor for atherosclerosis, and cellular senescence is associated with the proinflammatory phenotype of macrophages, which has been described as a senescence-associated secretory phenotype (SASP).[1–3] SASP is believed to play a vital role in

atherosclerosis.[4–6] We have already identified the critical role of 4 components of SASP in the form of (1) telomere shortening-triggered DNA damage and the subsequent p53 (tumor protein p53), p16 (cyclin-dependent kinase inhibitor 2A), and p21 (cyclin-dependent kinase inhibitor 1) induction; (2) reactive oxygen species (ROS) induction; (3) inflammation; and (4) impairment of efferocytosis during the process of atherosclerosis.[7] Senescence is characterized by cell cycle arrest, and therapy-induced senescence has long been a basis for cancer therapy to inhibit cancer cell growth.[8] However, this conventional view has recently been challenged.[9–11] Milanovic et al[10] reported that senescence reprograms cancer cells to acquire a proliferative phenotype (senescence-associated stemness [SAS]) after cancer therapy, which allows them to escape senescence-induced cell cycle arrest with strongly enhanced clonogenic growth potential. SAS is different from SASP and regulated independently of senescence-induced cell cycle arrest[12,13] and death.[14,15] It is now considered to be one of the critical mechanisms in developing resistance to cancer therapy.[14–16] Since both senescence and proliferation of macrophages[17] play critical roles in atherosclerotic plaque formation, we hypothesized that SAS could also be involved in atherosclerosis. However, to the best of our knowledge, SAS has not been explored in cardiovascular disease.

ERK5 (extracellular signal-regulated kinase 5; BMK1 [Big MAPK 1]/MAPK [mitogen-activated protein kinase] 7)—a member of the MAPK family—is unique in that it is not only a kinase but also a transcriptional coactivator with a long C-terminal transcriptional activation domain.[18,19] The ERK5 N-terminal kinase domain has a characteristic threonine-x-tyrosine (TEY) motif in the activation loop that activates both kinase and transcriptional activity once phosphorylated.[18] As a negative regulator of C-terminal transcriptional activation domain, once activated, the N-terminal kinase domain releases its inhibitory effect and activates C-terminal transcriptional activation domain. Both the association of ERK5 with transcriptional factors and the activation of ERK5 C-terminal transcriptional activation domain are required for transcriptional activation of MEF2 (myocyte enhancer factor 2),[20] PPARγ (proliferator-activated receptor γ),[18] and NRF2 (nuclear factor-erythroid factor 2 related).[21] We have reported that activated p90RSK (p90 ribosomal S6 kinase) binds the ERK5 C-terminal region (amino acids 571–807), enabling p90RSK to phosphorylate ERK5 S496[7] and inhibit the transcriptional activity of ERK5.[7] However, ERK5 kinase activation also can be upstream of p90RSK activation.[22] Importantly, ERK5 S496 phosphorylation is not dependent on ERK5 kinase activity.[1,7] p90RSK activation increased ERK5 S496 phosphorylation and induced atherosclerosis,[1] but the exact role and mechanisms of ERK5 S496 phosphorylation in atherosclerosis in vivo remain unclear. Also, oxidized LDL (low-density lipoprotein; oxLDL) can induce SASP in myeloid cells (MCs),[23] but how SASP is initiated by oxLDL has been incompletely characterized.

The effects of ERK5 in endothelial cells (ECs) and in the activation of monocytes on inflammation are controversial. Wilhelmsen et al[24] showed that ERK5 siRNA inhibits cytokine-induced inflammatory response in ECs and monocytes, whereas we found that depletion of ERK5 inhibits shear stress-induced anti-inflammatory effects in ECs.[18] Lin et al[25] generated a highly selective ERK5 kinase inhibitor (AX15836) and noted that unlike ERK5 depletion, AX15836 exerts no anti-inflammatory or antiproliferative effects. Lochhead et al showed that AX15836 induces KLF2 (Kruppel-like factor 2) transactivation; however, no data related to the effects of this inhibitor on inflammation or proliferation were provided.[26] All these differences indicate that ERK5-specific inhibitors might function differently from ERK5 genetic deletion or depletion. Lin et al[25] suggested that the phenotypes caused by ERK5 genetic depletion might be due to the removal of its noncatalytic function. However, it remains unclear what kind of noncatalytic function is removed by the deletion/depletion of ERK5 that can regulate anti-inflammatory or antiproliferation effects.

In this study, we evaluate the role of ERK5 S496 phosphorylation in the induction of atherosclerosis, SASP, and SAS in vivo in ERK5 S496A (dephosphorylation mimic) knock in (KI) mice, using a novel imaging mass cytometry (IMC) technique.[27] We also investigate whether ERK5 S496 phosphorylation inhibits NRF2 transcriptional activity via a noncatalytic function of ERK5 and its regulatory mechanism.

METHODS

Details of the experimental procedures are included in the Supplemental Material.

Data Availability

The RNA sequencing data were deposited in the National Center for Biotechnology Information (NCBI) Gene Expression Omnibus database (accession GSE210949). The data, analytic methods, and study materials that support the findings of this study are available in the Supplemental Material or from the corresponding authors upon reasonable request.

RESULTS

ERK5 S496 Phosphorylation Promotes Plaque Size and Vulnerable Plaque Formation

To determine the role of ERK5 S496 phosphorylation in atherosclerosis, we generated ERK5 S496A KI mice. We performed western blotting and confirmed that ERK5 S496 phosphorylation is absent but ERK1/2 and p90RSK are still activated in bone marrow–derived macrophages (BMDMs) isolated from ERK5 S496A KI mice (Figure 1A and 1B; Figure S1A). Conversely, we did not observe any changes in ERK5 TEY phosphorylation,

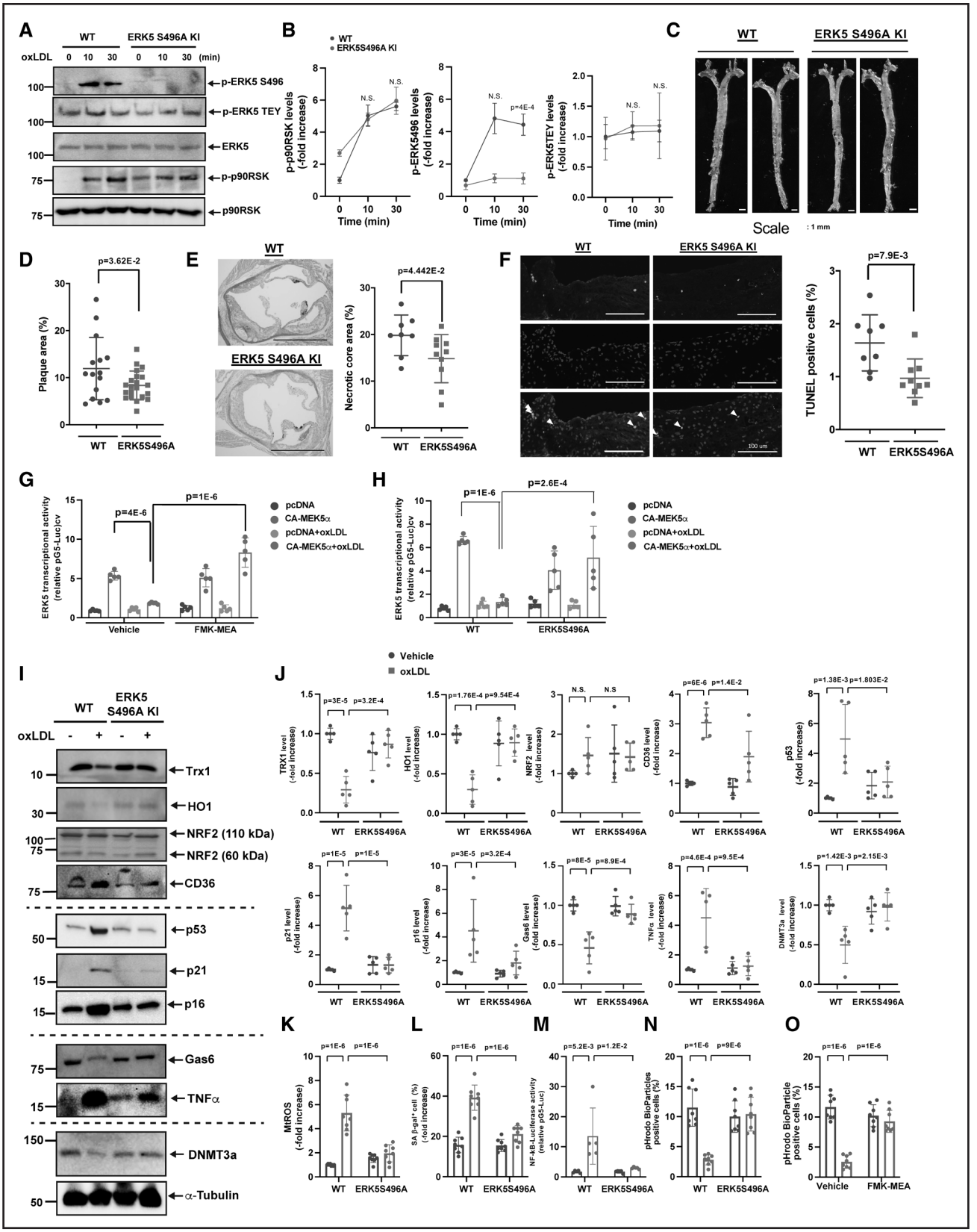

Figure 1. ERK5 (extracellular signal-regulated kinase 5) S496 phosphorylation plays a crucial role in vulnerable plaque formation and senescence-associated secretory phenotype (SASP) induction.

Wild type (WT) bone marrow–derived macrophages (BMDMs) and ERK5 S496A knock in (KI) BMDMs were treated with oxidized LDL (low-density lipoprotein; oxLDL; 10 μg/mL) for 0 to 30 minutes (**A** and **B**), and an immunoblotting analysis was performed using antibodies against the indicated proteins in vitro. **B**, The graphs represent densitometry data from 3 independent gels, one of which is shown in **A**. (*Continued*)

which represents ERK5 kinase activation, after oxLDL stimulation (Figure 1A and 1B). We fed ERK5 S496A KI and wild type (WT) C57BL6 control mice a high-fat diet (HFD) for 16 weeks after injecting all mice with a single dose of adeno-associated virus-8 overexpressing PCSK9 (proprotein convertase subtilisin/kexin type 9) gain-of-function D377Y mutant[34] as we reported previously. No differences in body weight, LDL, or HDL (high-density lipoprotein) cholesterol levels and cardiac function evaluated by echocardiography were noted (Figure S1), whereas the area of atherosclerotic lesions evaluated by oil red O staining in en face preparations of the ERK5 S496A KI aortas was smaller than that of the WT control aortas (Figure 1C and 1D). The size of necrotic cores (Figure 1E) and the percentage of terminal deoxynucleotidyl transferase dUTP nick end labeling–positive cells were decreased in ERK5 S496A KI aortas compared with that of the WT control aortas (Figure 1F), suggesting that ERK5 S496 phosphorylation increases atherosclerotic plaque size and promotes the formation of vulnerable plaques.

ERK5 S496 Phosphorylation Induces SASP Without Affecting ERK5 Catalytic Activity

OxLDL reduced a constitutively active form of MEK5 (MAPK/ERK Kinase 5)-induced ERK5 transcriptional activity detected by luciferase reporter assay, which could be reversed by FMK-MEA, a specific inhibitor of p90RSK[7] (Figure 1G), and in BMDMs isolated from ERK5 S496A KI mice (Figure 1H). However, oxLDL showed no significant effects on baseline ERK5 transcriptional activity in the MCs transfected with the control plasmid (empty pcDNA without constitutively active form of MEK5). Next, we examined the effects of ERK5 S496 phosphorylation on the following 4 SASP characteristics: (1) excessive ROS production with reduction of antioxidants, (2) senescence, (3) reduction of efferocytosis, and (4) proinflammation.[1] Although oxLDL showed no effect on baseline ERK5 transcriptional activity (Figure 1G), it decreased the expression of antioxidant molecules such as TRX1 (thioredoxin 1) and HO1 (heme oxygenase 1); this decrease was completely reversed in BMDMs isolated from ERK5 S496A KI mice (Figure 1I and 1J). We also found that oxLDL increased mitochondrial ROS (mtROS) production in WT BMDMs, which was inhibited in ERK5 S496A KI BMDMs as detected by 2 separate MitoNeoD and MitoSOX red assays as described in the Methods (Figure 1K [MitoNeoD]; Figure S1F and S1G [MitoSOX]). OxLDL increased expression of p16, p21, and p53 detected by western blotting (Figure 1I and 1J) and induced SA-βgal (senescence-associated β-gal) staining (Figure 1L), all of which were absent in ERK5 S496A KI BMDMs. GAS6 (growth arrest-specific protein 6) and DNA damage response–related molecule DNMT3a (DNA methyltransferase 3a) expression was inhibited, but TNFα (tumor necrosis factor alpha) was increased by oxLDL in WT BMDMs (Figure 1I and 1J). In WT BMDMs, oxLDL increased NF-κB (nuclear factor kappa B) activation (Figure 1M) while reducing efferocytosis detected by using pHrodo dye[27] (Figure 1N and 1O); all of these effects observed in WT BMDMs were reversed in ERK5 S496A KI BMDMs or by FMK-MEA (Figure 1N and 1O). Of note, oxLDL had no effect on both ERK5 kinase activity and transcriptional activity (Figure 1A, 1G, and 1H). These data suggest that ERK5 S496 phosphorylation regulates SASP independent of ERK5 catalytic activity.

Divergent Role of ERK5 S496 Phosphorylation in SASP in MCs and ECs

IMC is a technique that uses antibodies conjugated with rare-earth-metal isotopes of defined atomic

Figure 1 Continued. **C** and **D**, Sixteen weeks after adeno-associated virus (AAV)–PCSK9 (proprotein convertase subtilisin/kexin type 9) injection and being fed a high-fat diet (HFD), ERK5 S496A KI mice exhibited fewer oil red O–stained atherosclerotic lesions in the en face whole aorta; scale bars, 1 mm. **D**, Quantified oil red O–stained lesions are shown (n=15 and 21; all male). **E**, The area occupied by the necrotic core (acellular lipid core) is shown as the percentage of the total lesion area (**E**, **right**). Scale bar, 1 mm (n=8 and 10). **F**, Sections of proximal aortas from each group were labeled using terminal deoxynucleotidyl transferase dUTP nick end labeling (TUNEL) reagents to detect apoptotic cells and counterstained with 4′,6-diamidino-2-phenylindole (DAPI) to detect nuclei. Only double-positive cells (TUNEL and DAPI) were counted. Scale bar, 100 μm. **F**, **Right**, The graph shows the percentage of TUNEL-positive cells (TUNEL+ cells/total cells counted) in the lesion area. Over 200 cells were counted for each group (n=8 and 9). **G** and **H**, BMDMs treated with vehicle or FMK-MEA (**G**) or WT BMDMs and ERK5 S496A KI BMDMs (**H**) were incubated with oxLDL (10 μg/mL) or vehicle, and ERK5 transcriptional activity was detected. **I** and **J**, WT BMDMs and ERK5 S496A KI BMDMs were treated with oxLDL (10 μg/mL) for 24 hours, and immunoblotting analysis was performed using antibodies against the indicated proteins in vitro. **J**, The graphs represent densitometry data from 5 independent gels, one of which is shown in **I**. **K**, WT BMDMs and ERK5 S496A KI BMDMs were incubated with oxLDL as indicated. mitochondrial reactive oxygen species (mtROS) levels were detected by MitoNeoD as described in Methods. Cells treated with oxLDL were assayed 24 hours later. **L**, The percentages of cells positive for SA-βgal (senescence-associated β-gal) staining are shown in vitro. More than 200 cells per sample were counted. **M**, WT BMDMs and ERK5 S496A KI BMDMs were transfected with the NF-κB (nuclear factor kappa B) luciferase reporter and the constitutively expressing *Renilla* luciferase vector for 16 hours and then incubated with oxLDL or vehicle. After 12 hours, NF-κB transcriptional activity was measured as described in Methods in vitro. **N** and **O**, BMDMs treated with vehicle or fluoromethyl ketone–methoxyethylamine (FMK-MEA; 10 μM; **N**) or WT BMDMs and ERK5 S496A KI BMDMs (**O**) were incubated with oxLDL (10 μg/mL) or vehicle. After 24 hours, pHrodo-positive cells were quantified in vitro. The applied statistical tests, sample number, and results in all figures are summarized in Table S3. All data are expressed as mean±SD; $^{**}P<0.01$, $^{*}P<0.05$.

masses that allows the antibody-bound proteins to be separated by a mass cytometer instead of fluorescent or enzymatic moieties that are used in conventional immunohistochemistry and immunohistofluorescence. We prepared tissue sections from the plaques of the WT mice fed an HFD (WT HFD) and the ERK5 S496A KI mice fed an HFD (ERK5 S496 KI HFD) or a normal chow diet (NCD) as a control for 12 weeks after adeno-associated virus-8 overexpressing PCSK9 gain-of-function D377Y mutant injection and then generated high-dimensional images of these tissue sections (Figure 2A and 2B, top). Using the VISIOPHARM program (Hoersholm, Denmark), single-cell features were computationally segmented by a watershed algorithm (Figure 2B, bottom). Single-cell markers or molecule expression data were extracted and analyzed by the Phenomap module, and t-SNE plots were generated by a phenotyping algorithm (Figure 2D). Based on these analyses, we found 9 clusters in both WT and ERK5 S496A KI plaques (Figure 2C and 2E). Using CD31, von Willebrand factor, and ETS (erythroblast transformation-specific) transcription factor ERG-related genes as EC markers and cluster of differentiation (CD)11b and CD107b as MC markers, we identified 2 EC-like clusters (No. 5 and 6) and 5 MC-like clusters (No. 1, 3, and 7–9; Figure 2C and 2E). No statistically significant difference in the relative cellularity (percentage of total cells) of these clusters between WT and ERK5 S496A KI plaques was observed (Figure 2F).

In 5 MC-like clusters (No. 1, 3, and 7–9), we found less expression of p53 and more expression of TRX1 in clusters 3 and 7, DNMT3a in clusters 7 and 8, TYRO3 (tyrosine-protein kinase receptor TYRO3) in cluster 7, and GAS6 and TOP2β (DNA topoisomerase IIβ) in cluster 9 in ERK5 S496A KI plaques compared with WT plaques (Figure 2G through 2O). We also verified the IMC findings using immunohistochemistry and found a decreased expression of p53 in macrophages (LAMP2 [lysosomal associated membrane protein 2; also known as Mac3]-positive cells [demarcated area]) and an increased expression of TRX1 and DNMT3a in ERK5 S496A KI plaques compared with WT plaques (Figure S2A through S2C). These data suggest that the SASP-related events, including p53, efferocytosis (TYRO3), antioxidation (TRX1), and DNA damage response (TOP2β), are regulated by ERK5 S496 phosphorylation in MCs localized in the atherosclerotic plaques in vivo.

In the 2 EC-like clusters, the intensity of signals associated with the SASP events was weaker than that in the 5 MC-like clusters. However, we still found an increased expression of TRX1, GAS6, TYRO3, and DNMT3A in ERK5 S496A KI plaques compared with WT plaques (Figure S2D). Alternatively, we did not detect any differences in the expression of p53 and TOP2β in EC-like clusters between ERK5 S496A KI plaques and WT plaques (Figure S2D). Interestingly, IL (interleukin)-6 expression was higher in MC-like clusters (No. 1, 7, and 9) and EC-like cluster (No. 5) in ERK5 S496A KI plaques than in those of the WT plaques (Figure 2M; Figure S2D). IL-6 atheroprotective effects may contribute to less plaque formation in ERK5 S496A KI mice.[28]

Since the distribution of MCs in relation to blood vessels can provide information about macrophage infiltration and migration to the plaque, we performed a morphometric analysis of the distance between MCs and ECs in WT and ERK5 S496A KI plaques. Although matching plaque sizes were selected for analysis, the mean distance from the EC-like cluster 5 to the MC-like cluster 8 was shorter in ERK5 S496A KI plaques than in WT plaques (Figure S2E). We also found that the migration of ERK5 S5496A KI BMDMs detected by Boyden chamber assay was significantly less than WT (Figure S2F). These data indicate that ERK5 S496 phosphorylation promotes MC-like cell infiltration and migration.

ERK5 S496 Phosphorylation Promotes SAS

Milanovic et al[10] have defined SAS as "an unexpected, cell-autonomous feature that exerts its detrimental, highly aggressive growth potential upon escape from the cell-cycle blockade." p53 plays a crucial role in controlling senescence-induced cell cycle arrest,[29] especially in macrophages during atherosclerosis formation.[30] IMC data analysis shows that p53 is expressed at relatively higher level among all senescent markers tested (Figure S2G). To determine whether senescence, particularly SAS, is induced during the process of atherosclerosis, we investigated the relationship between p53 and Ki67 (as a proliferation marker in the atherosclerosis lesions[31]) in the plaques in vivo by calculating the logarithm of the Ki67 expression to p53 expression ratio at a single-cell level ($\log_{10}$[Ki67:p53] ratio of selected cells) in IMC data. Because the 1-dimension density distribution of this parameter was trimodal, MCs were divided into 3 groups based on different patterns of p53:Ki67 expression (Figure 3A) with the cutoff values −1.01 and −0.024 (Figure 3B). Antiproliferative effects of p53 appear to explain the Ki67:p53 ratio in MC groups 1 and 3; however, p53 and Ki67 were linearly coexpressed in group 2 (y=0.92x+0.81; F test, P value, $<2.2\times10^{-16}$), indicating that this group likely escaped from antiproliferative effects of p53 (Figure 3A). Quantitative data analysis showed the percentage of ERK5 S496A KI cells in group 2 was lower than that of the WT cells (Figure 3D). In contrast, the percentage of ERK5 S496A KI cells in group 3 was higher than that of the WT cells and was not different from that of the WT cells in MC group 1 (Figure 3C and 3E). Collectively, these data implicate a unique role of ERK5 S496 phosphorylation in regulating SAS in MCs during atherogenesis.

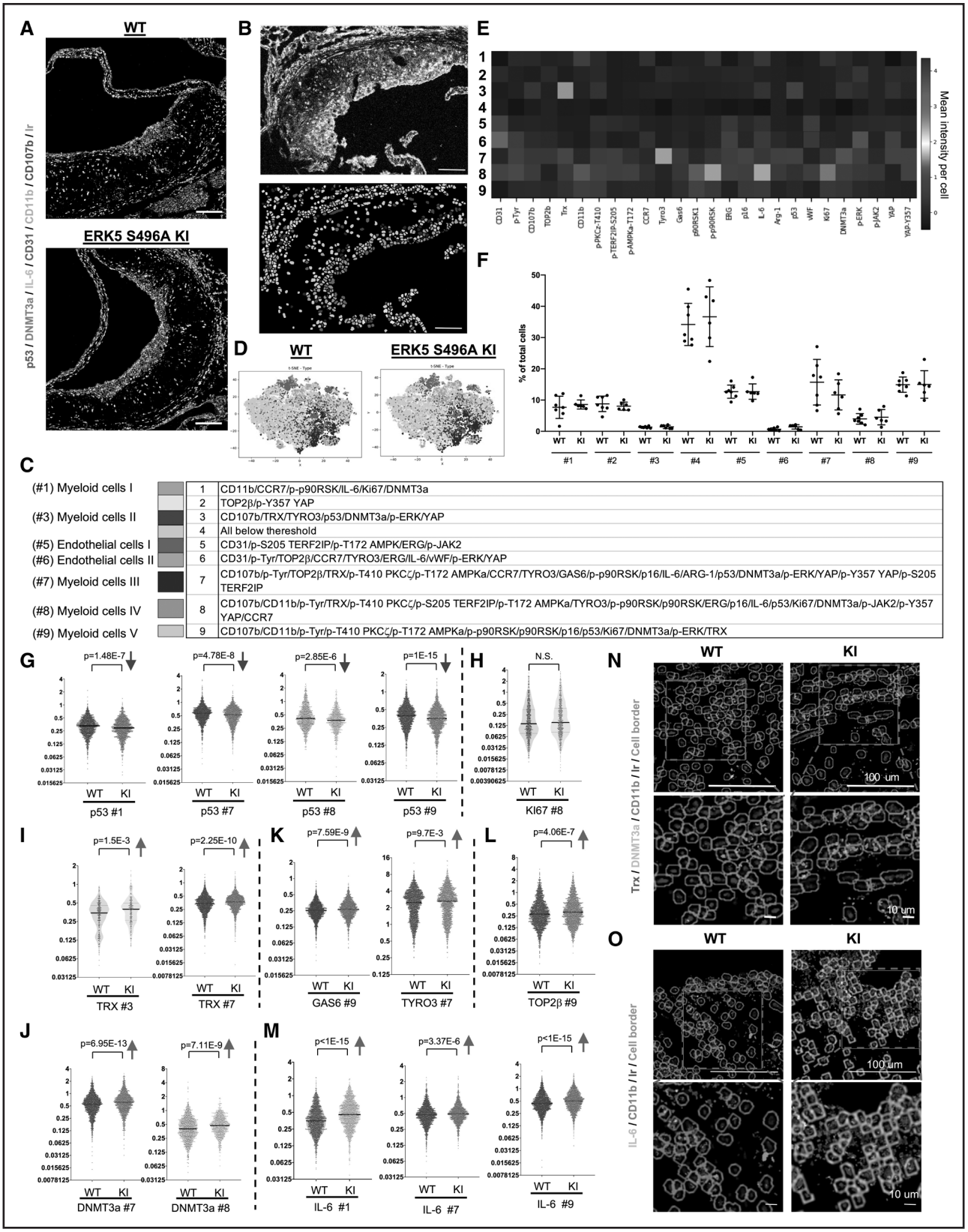

Figure 2. Single-cell–based clustering by imaging mass cytometry and senescence-associated secretory phenotype (SASP) markers in wild type (WT) and ERK5 (extracellular signal-regulated kinase 5) S496A knock in (KI) plaques in vivo.
A, Six transient and single isotope signals from the markers and the Ir DNA-intercalator signal were plotted. **B**, **Top**, Imaging mass cytometry (IMC) analysis of tissues sectioned from WT and ERK5 S496A KI plaques. All 26 transient and single isotope signals from the markers and the Ir DNA-intercalator signal were plotted. **B**, **Bottom**, and **C**, After cell segmentation and phenotyping, 9 phenotypic clusters were (*Continued*)

In contrast to MCs, we could not find the apparent SAS phenotype in ECs (Figure S2I). We also performed IMC analysis with vascular smooth muscle cells (VSMCs) by using α-SMA (α-smooth muscle actin) antibody and found group 1 (high p53 and low Ki67) and group 3 (low p53 and high Ki67) phenotypes, but VSMCs did not show SAS phenotype of group 2 (the linear relationship between p53 and Ki67 expression; Figure S2J). We also evaluated the SASP phenotype in VSMCs and found an upregulation of DNMT3a and GAS6 expression in VSMCs from the plaque of ERK5 S496A KI mice. However, we could not find other SASP molecules changes between WT and ERK5 S496A KI mice in VSMCs (Figure S2K). These data indicate that the SAS phenotype was present in MCs, but it was less clear in ECs and VSMCs.

Hypercholesterolemia Induces MC Phenotypic Changes to SASP/SAS via ERK5 S496 Phosphorylation

Although cell cycle arrest is a hallmark of senescence, senescent cells can escape cell cycle arrest and acquire the SAS phenotype.[10] Since MC proliferation is a crucial component of plaque formation,[17] SAS can play a critical role in atherosclerosis. We demonstrated the potential existence of SAS in the plaque (Figure 3A through 3E). To investigate how SAS was regulated in MCs by hypercholesterolemia, we isolated bone marrow cells from WT and ERK5 S496A KI mice fed an HFD or NCD for 16 weeks after adeno-associated virus–PCSK9 gain-of-function D377Y mutant injection and differentiated them to BMDMs for evaluation of SASP and SAS induction.

We found (1) an increase of p53, p21, and p16 and SA-βgal–positive cells (Figure 3F and 3G; Figure S3); (2) a decrease of TRX1 and HO1 (Figure 3F; Figure S3); an increase of mtROS (Figure 3H [MitoNeoD]; Figure S1G [MitoSOX]); (3) a decrease of GAS6 (Figure 3F; Figure S3) and efferocytosis (Figure 3I); and (4) an increase of TNFα and various cytokine and chemokine secretion (Figure 3F; Figure S3 and S4) in BMDMs isolated from hypercholesterolemic WT HFD mice compared with that of normocholesterolemic WT NCD mice were inhibited in BMDMs isolated from hypercholesterolemic ERK5 K496A KI HFD mice. We also found an increase in arginase-1 and Fizz1 mRNA in BMDMs isolated from hypercholesterolemic ERK5 S496A KI HFD mice (Figure S4B), suggesting the shift from M1- to an M2-like phenotype in MCs by the ERK5 S496A mutation. Furthermore, levels of IL-1α, IL-1β, and CXCL3 (C-X-C motif chemokine ligand 3) cytokines in serum obtained from ERK5 S496A KI HFD mice were lower than those from WT HFD mice (Figure S4C), also supporting the role of ERK5 S496 phosphorylation in SASP induction.

Because mitochondrial dysfunction plays a critical role in the induction of SASP,[32] we examined oxidative phosphorylation and glycolysis in cultured BMDMs isolated from WT or ERK5 S496A KI mice after NCD or HFD. Whereas oxidative phosphorylation was decreased, glycolysis was increased in BMDMs from hypercholesterolemic WT HFD mice compared with normocholesterolemic WT NCD mice—an effect that was completely reversed in BMDMs from ERK5 S496A KI mice (Figure S5). OxLDL reduced the ATP and nicotinamide adenine dinucleotide levels in WT BMDMs but not in ERK5 S496A KI BMDMs (Figure 3J and 3K).

Since the data in Figure 3F through 3K supported the idea that BMDMs from NCD and HFD-fed mice showed significant phenotypic differences in SASP, we also evaluated 2 senescence markers (53BP1 [p53-binding protein 1] and LMNB1 [lamin B1]) and cell growth marker (PCNA [proliferating cell nuclear antigen]) as evidence for SAS in hypercholesterolemic-mediated reprogrammed BMDMs. We observed an increase of 53BP1 and PCNA and a decrease of LAMIN B1 expression in hypercholesterolemic WT HFD mice (HFD BMDMs) compared with normocholesterolemic WT NCD mice (NCD BMDMs)—an effect that was reversed in ERK5 S496A KI BMDMs (Figure 3F;

Figure 2 Continued. identified in WT and ERK5 S496A KI plaque tissues. Each color indicates a cell cluster in **C**. **D**, t-distributed stochastic neighbor embedding (t-SNE) plots of WT and ERK5 S496A KI plaque tissues. **E**, Heat map with 9 phenotypic clusters showed differentially regulated 26 molecules. **F**, Cell number (%) in each cluster of total cells in each region of interest (ROI). We measured 18 ROIs from 7 WT samples and 18 ROIs from 6 ERK5 S496A KI samples and averaged the values from the same sample (n=7 and 6). Data are expressed as mean±SD. Statistical significance was assessed by 1-way ANOVA and showed no difference between WT and ERK5 S496A KI. **G**–**M**, The single-cell expression level of each marker in MC-like clusters between WT and ERK5 S496A KI plaque tissues. p53 expression levels in #1, #7, #8, and #9 were decreased in ERK5 S496A KI cells compared with those in WT cells (**G**). Ki67 expression in the most inflammatory MC-like cluster (No. 8) was not changed between WT and ERK5 S496A KI cells (**H**). TRX expression levels in #3 and #7; DNMT3a in #7 and #8; TYRO3 (tyrosine-protein kinase receptor TYRO3) in #7; GAS6 (growth arrest-specific protein 6) and TOP2β (DNA topoisomerase IIβ) in #9; and IL (interleukin)-6 in #1, #7, and #9 were increased in ERK5 S496A KI cells compared with those in WT cells (**I**–**M**). The *y* axis indicates the mean intensity, and solid black lines indicate the median value in each violin plot. **N** and **O**, Staining images of each marker acquired by IMC were exported by the MCD viewer and merged with cell border images (gray) exported from VIS software. Ir (blue) is DNA. **Top**, Low magnification (scale bar, 100 μm). **Bottom**, High magnification (scale bar, 10 μm). **N**, Trx (magenta) and DNMT3a (yellow) in CD11b (lime)-positive myeloid cells were induced in ERK5 S496A KI compared with WT cells. **O**, IL-6 (yellow) in CD11b (lime)-positive myeloid cells was induced in ERK5 S496A KI compared with WT cells. The applied statistical tests, sample number, and results in all figures are summarized in Table S3. CD indicates cluster of differentiation.

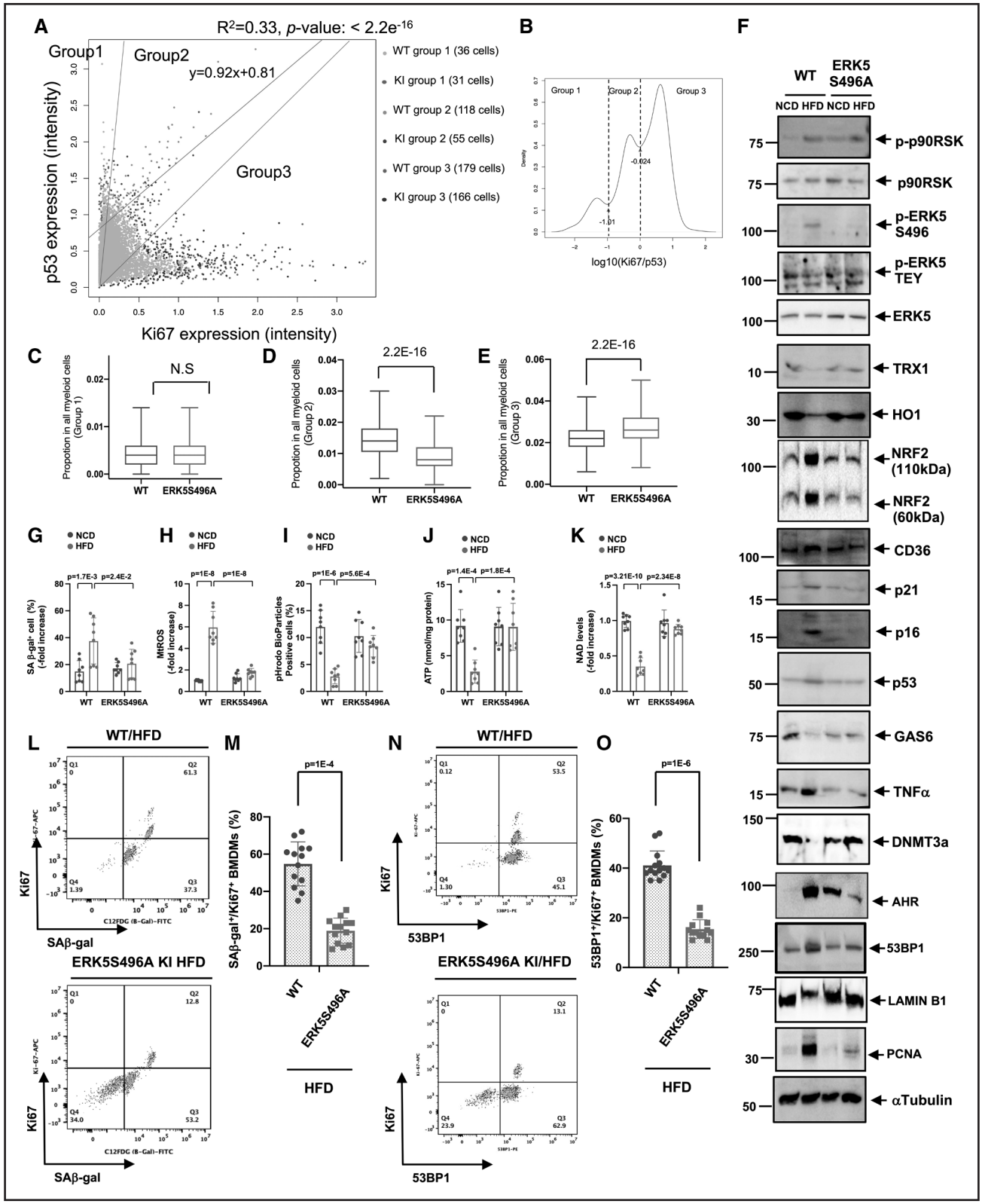

Figure 3. ERK5 (extracellular signal-regulated kinase 5) S496 phosphorylation provokes senescence-associated stemness (SAS) in vivo and ex vivo.

A–**E**, Single-cell analysis of p53 and Ki67 expression in vivo. **B**, The log scaled ratio of Ki67 and p53 of selected cells by $\log_{10}$(expression of Ki67/expression of p53), and the cutoff of ratio with $\log_{10}(-1.01)$ and $\log_{10}(-0.024)$. **C**–**E**, The percentage of ERK5 S496A knock in (KI) cells in groups 1 to 3. KI and wild type (WT) cells were resampled for 1000 rounds to calculate the percentage of cells in groups 1 to 3. In each resampling round, 500 KI (or WT) cells were selected to calculate the percentage in group 1 (or group 2 or 3) by number of cells in group 1 (or group 2 or 3)/number of total cells. Wilcoxon test was performed as described in the Methods. **F**–**O**, Bone (*Continued*)

Figure S3). Furthermore, we examined the amount of double SAβ-gal and Ki67 positive (SA β-gal$^+$Ki67$^+$; Figure 3L and 3M) and double 53BP1 and Ki67 positive (53BP1$^+$Ki67$^+$) macrophages (Figure 3N and 3O) and found a significant decrease of both SA β-gal$^+$Ki67$^+$ and 53BP1$^+$Ki67$^+$ macrophages obtained from hypercholesterolemic ERK5 S496A KI HFD mice compared with those from the hypercholesterolemic WT HFD mice (Figure 3L through 3O). These data indicate that SAS is increased in hypercholesterolemic-mediated reprogrammed MCs in an ERK5 S496 phosphorylation-dependent manner.

AHR Is Required for ERK5 S496 Phosphorylation-Induced SAS

To investigate the molecular mechanism by which ERK5 S496 phosphorylation reprograms MCs to SAS, we performed RNA sequencing for WT and ERK5 S496A KI BMDMs under NCD or HFD. We identified 784 differentially expressed genes regulated only by hypercholesterolemic-induced ERK5 S496 phosphorylation (Figure 4A through 4C). The gene ontology analysis revealed that these differentially expressed genes are involved in critical senescence-related processes such as cell cycle, cellular response to DNA damage, protein transport, and negative regulation of apoptosis (Figure 4D; Figure S6). Gene ontology bubble analysis showed the strong involvement of ERK5 S496 phosphorylation in nuclear events, also supporting its role in regulating senescence events (Figure S6). Gene annotation enrichment analysis (GO Circle) showed that *Z* scores of both cell cycle and cellular response to DNA damage were negative in ERK5 S496A KI (Figure 4D and 4E), suggesting the role of cell cycle and DNA damage response in inducing SAS. Interestingly, we found only 30 differentially expressed genes between WT NCD and WT HFD BMDMs (Figure 4F), among which 15 differentially expressed genes were regulated by ERK5 S496 phosphorylation (Figure 4G and 4H). These observations support the critical role of ERK5 S496 phosphorylation in hypercholesterolemic-mediated MC reprogramming. We identified 10 core genes (*Ahr*, *Gclm*, *H3C3*, *H4c11*, *Lpar1*, *Megf9*, *Nfe2*, *Ppih*, *Rpl22l1*, and *Tpt1*) regulated by hypercholesterolemic-mediated ERK5 S496 phosphorylation that might be crucial for hypercholesterolemic-induced SAS.

Since *Ahr* showed the most significant changes among the 10 core genes, and its contribution to both cell proliferation[33] and senescence[34] had already been reported, we next investigated its expression in BMDMs. We found an increase in AHR (aryl hydrocarbon receptor) protein expression in WT HFD compared with WT NCD BMDMs ex vivo. This increase was no longer apparent in ERK5 S496A KI HFD BMDMs (Figure 3F; Figure S3). In addition, NRF2-KEAP1 (kelch like ECH associated protein 1)–binding inhibitory peptide (NRF2A) inhibited AHR expression (Figure 4I) in BMDMs of WT HFD mice. The depletion of AHR inhibited the increase of SAβ-gal$^+$Ki67$^+$ macrophages in WT HFD BMDMs (Figure 4J and 4K), supporting the pivotal role of AHR in hypercholesterolemic-induced SAS.

ERK5 S496 Phosphorylation, but Not ERK5 Catalytic Activity, Is Crucial for Inflammation and mtROS Induction

Since we did not find an increase in ERK5 TEY motif phosphorylation by oxLDL (Figure 1A), we used GM-CSF (granulocyte-macrophage colony-stimulating factor) to detect ERK5 TEY motif phosphorylation. We transfected BMDMs with an ERK5b splice variant cDNA mutant (aa78-806), which lacked an ATP-binding site and showed no ERK5 kinase or transcriptional activity.[18,35] We also studied the effect of a dual phosphorylation site mutant of ERK5 (ERK5TEYm), which inhibited stimuli-induced ERK5 kinase activation[36] after TEY motif phosphorylation (Figure 5A). In BMDMs transfected with the ERK5b or the ERK5TEYm, GM-CSF–induced ERK5 TEY motif phosphorylation and the subsequent KLF2 induction were inhibited, whereas ERK5 S496 phosphorylation was unaffected (Figure 5B and 5C; Figure S7A and S7B). In contrast, ERK5 kinase inhibitor XMD8-92 and the highly selective ERK5 kinase inhibitor AX-15836[25] both suppressed ERK5 TEY motif phosphorylation–mediated KLF2 induction and S496 phosphorylation (Figure 5D and 5E; Figure S7C and S7D). Lastly, the ERK5 S496A mutant inhibited ERK5 S496 phosphorylation but had no effect on KLF2 induction

Figure 3 Continued. marrow–derived macrophages (BMDMs) isolated from WT and ERK5 S496A KI mice fed a normal chow diet (NCD) or high-fat diet (HFD) for 4 months were cultured with the same medium ex vivo. **F**, Immunoblotting analysis was performed using antibodies against the indicated proteins. We used the α-tubulin expression as a loading control for each protein (quantification data are shown in Figure S3). **G**, The percentages of cells positive for SA-β-gal (senescence-associated β-gal) staining are shown. **H**, Mitochondrial reactive oxygen species (mtROS) levels were detected by MitoNeoD as described in Methods. **I**, Efferocytosis was detected by the quantification of pHrodo-positive cells (%). ATP (**J**) and NAD$^+$ (**K**) were measured in BMDMs isolated from WT and ERK5S496A KI mice fed an NCD or HFD. **L**, Coexpression of the fluorescent SA-β-gal marker and Ki67 in BMDMs isolated from WT and ERK5 S496A KI mice after 4 months of HFD. **M**, The graph showed the percentage of double-positive SA-β-gal and Ki67 cells. **N**, Coexpression of the fluorescent 53BP1 (p53-binding protein 1) marker and Ki67 in BMDMs isolated from WT mice after 4 months of HFD. **O**, The graph showed percentage of double-positive 53BP1 and Ki67 cells. n=13 to 14. The applied statistical tests, sample number, and results in all figures are summarized in Table S3. All data are expressed as mean±SD; $^{**}P<0.01$, $^{*}P<0.05$.

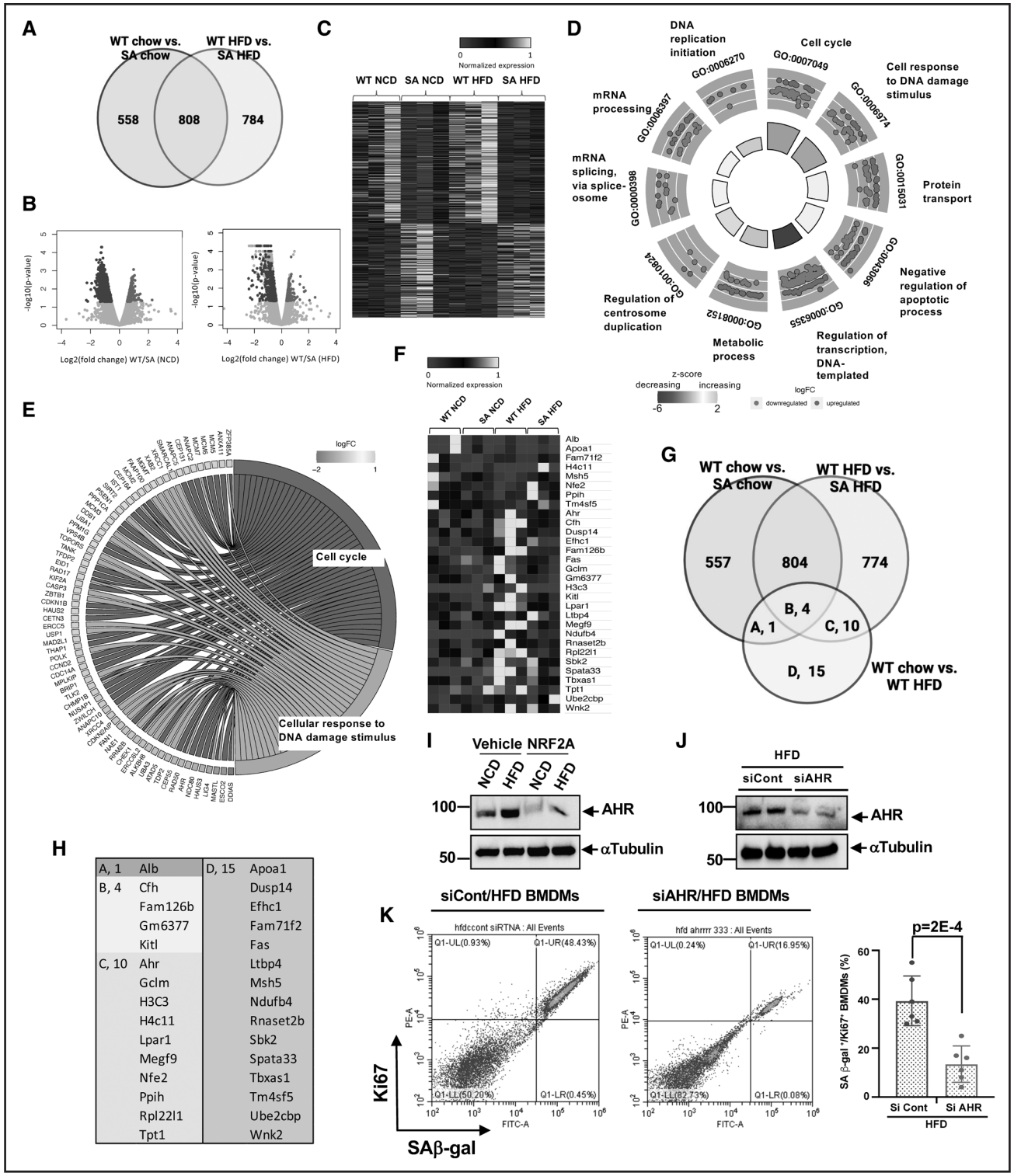

Figure 4. ERK5 (extracellular signal-regulated kinase 5) S496 phosphorylation regulates the genetic profile of hypercholesterolemic (HC)-mediated reprogrammed MCs and the critical role of AHR (aryl hydrocarbon receptor) on senescence-associated stemness (SAS) ex vivo.

A, Venn diagram illustrating the gene expression patterns in each experimental group. **B**, Volcano plot of bone marrow–derived macrophages (BMDMs) from wild type (WT) and ERK5 S496A knock in (KI) fed a normal chow diet (NCD) or high-fat diet (HFD) RNA sequencing adjusted *P* value <0.01, 1039 genes upregulated and 327 downregulated in WT versus SA NCD, and 1174 genes upregulated and 418 downregulated in WT versus SA HFD. Three samples per group. **C**, Heat map differentially regulated 784 genes only between WT HFD and ERK5 S496A KI HFD (SA HFD). **D**, Functional enrichment analyses. GO Circle plots display scatter plots of log fold change (logFC) for selected gene ontology terms. Red dots represent upregulated genes, and blue dots represent downregulated genes. The inner circles display *Z* scores calculated as the number of upregulated genes minus the number of downregulated genes divided by the square root of the count for a WT HFD (*Continued*)

mediated by ERK5 TEY phosphorylation (Figure 5F; Figure S7E). These data support the crucial role of ERK5 TEY motif phosphorylation, but not ERK5 S496 phosphorylation, in ERK5 kinase activation–mediated KLF2 induction.

ERK5 kinase inhibitors prevented oxLDL-mediated ERK5 S496 phosphorylation and TNFα induction but showed no effect on p90RSK phosphorylation (Figure 5H and 5I; Figure S7H and S7I), which supports the specificity of ERK5 kinase inhibitors. In contrast, ERK5b did not inhibit oxLDL-mediated p90RSK phosphorylation, ERK5 S496 phosphorylation, and TNFα induction (Figure 5G; Figure S7G). These data indicate that the inhibition of ERK5 catalytic activity is dispensable for the anti-inflammatory effects of ERK5 kinase inhibitors. Interestingly, ERK5TEYm inhibited both oxLDL-induced p90RSK phosphorylation and TNFα induction (Figure 5J; Figure S7F), indicating a unique role for ERK5 TEY motif phosphorylation on interplay between ERK5 and p90RSK, which could subsequently regulate p90RSK activation in an ERK5 kinase activity–independent manner.[37]

Lastly, we found that both ERK5b deletion mutant and ERK5TEYm could not inhibit oxLDL-induced mtROS production, but ERK5 S496A and both ERK5 kinase inhibitors inhibited mtROS production (Figure 5K; Figure S1H). Taken together, this finding indicates a crucial role for ERK5 S496 phosphorylation in mtROS production, independent of ERK5 catalytic activity.

ERK5 S496 Phosphorylation Induces NRF2 SUMOylation to Provoke SASP and Mitochondrial Dysfunction

OxLDL-induced reduction of NRF2 transcriptional activity detected by luciferase reporter assay was abolished by ERK5 S496A mutant and AX15836 but not by the ERK5b deletion mutant (Figure 6A). The data collectively (Figure 5K; Figure S1I) suggest that ERK5 kinase inhibitors might inhibit oxLDL-mediated reduction of NRF2 transcriptional activity and subsequent mtROS induction by inhibiting ERK5 S496 phosphorylation but not ERK5 catalytic activity. The role of SUMOylation in the regulation of transcriptional factor activity has already been reported.[38] We investigated whether NRF2 SUMOylation can be regulated by ERK5 S496 phosphorylation. OxLDL-increased NRF2 SUMOylation in WT BMDMs was inhibited in ERK5 S496A KI BMDMs (Figure 6C). Importantly, we also found an increase of NRF2 SUMOylation in WT HFD compared with WT NCD BMDMs but not in ERK5 S496A KI BMDMs (Figure S8A and S8B). NRF2 SUMOylations at K525(6)/595(6)[39] and K110[40] (NXQ16236-1) have been reported (Figure 6B). However, based on iPTMnet (No. Q16236)—the publicly accessible posttranslational modification database—only K518 is an NRF2 SUMOylation site detected by mass spectrometry,[41] and to the best of our knowledge, the functional role of NRF2 K518 SUMOylation remains unclear. Therefore, we generated the NRF2 K518R mutant and found that the NRF2 K518 to R mutation blocked oxLDL-induced NRF2 SUMOylation, indicating that NRF2 K518 is a primary SUMOylation site in MCs in response to oxLDL stimulation (Figure 6D). Next, we found that the inhibition of NRF2 transactivation after oxLDL treatment was reversed by NRF2 K518R mutant, indicating that NRF2 K518 SUMOylation inhibited NRF2 transcriptional activity (Figure 6E). All 4 components of SASP were abolished by transfection with the NRF2 K518R mutant (Figure 6F through 6J; Figure S8C). Furthermore, we also found that the NRF2 K518R mutant negated the oxLDL-induced AHR expression (Figure 6J; Figure S8C).

Mitochondrial dysfunction plays a crucial role in triggering SASP.[32] Whereas levels of oxidative phosphorylation, ATP, and nicotinamide adenine dinucleotide were decreased, glycolysis was increased in WT BMDMs after oxLDL incubation; however, these effects were attenuated in ERK5 S496A KI BMDMs (Figure 7A through 7F). Although oxLDL effects on glycolysis after plasmid transfection were less clear, we observed a decreased oxidative phosphorylation, ATP, and nicotinamide adenine dinucleotide after adding oxLDL to the cells overexpressing NRF2 WT; however, this decrease was no longer apparent in cells with the NRF2 K518R mutant (Figure 7G through 7L). Taken together, these observations indicate a critical role of NRF2 K518 SUMOylation in SASP/SAS and AHR induction.

DISCUSSION

In this study, we have used ERK5 S496A KI mice to show a decrease in the size of atherosclerosis and vulnerable plaque formation with the reduction of necrotic core formation and apoptotic cell accumulation in

Figure 4 Continued. and ERK5 S496A KI HFD. Upregulated means that expression is higher in the ERK5 S496A KI HFD. **E**, Circle plot of select genes indicated ontologies. Gene expression relative difference (log_2 fold change). **F**, Heat map differentially regulated 30 genes only between WT NCD and WT HFD (WT HFD). **G**, Venn diagram including the genes listed in **E**. **H**, The list of genes. **I**, AHR expression in BMDMs from WT fed an NCD or HFD after 24 hours of the vehicle or NRF2 (NFE2-related factor 2)-KEAP1 (kelch like ECH associated protein 1)–binding inhibitory peptide, CAS 1362661 (NRF2A; 2 μM) treatment. **J**, AHR expression in BMDMs from WT fed an HFD after AHR siRNA or control siRNA transfection. **K**, Coexpression of the fluorescent SA-β-gal (senescence-associated β-gal) marker and Ki67 in BMDMs isolated from WT HFD after transfection of control siRNA and AHR siRNA graph showed percentage of double-positive cells of SA-β-gal and Ki67. The applied statistical tests, sample number, and results in all figures are summarized in Table S3. Mean±SD; $^{**}P<0.01$.

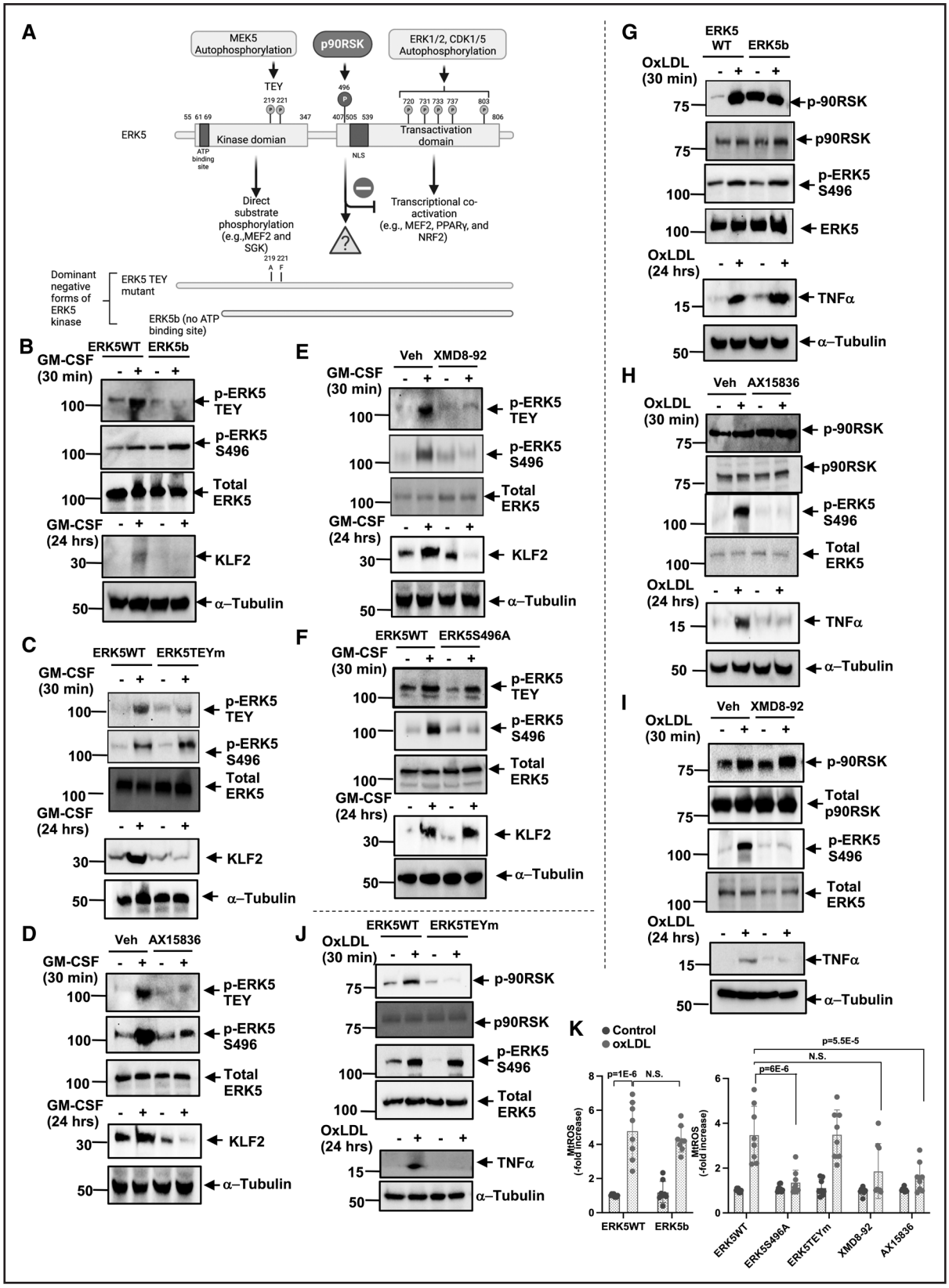

Figure 5. ERK5 (extracellular signal-regulated kinase 5) threonine-x-tyrosine (TEY) motif mutant and ERK5-specific kinase inhibitors inhibited ERK5 kinase activity and ERK5 S496 phosphorylation in vitro.

A, The scheme of ERK5 kinase, transactivation domain, and phosphorylation sites. Bone marrow–derived macrophages (BMDMs) were transfected with ERK5 wild type (WT) or ERK5b (**B** and **G**), ERK5 TEY motif mutant (ERK5TEYm; **C** and **J**), ERK5 S496A mutant (**F**), or pretreated with AX15836 (**D** and **H**; 5 μM), XMD8-92 (**E** and **I**; 10 μM), or vehicle for 1 hour, then BMDMs were stimulated by (*Continued*)

response to hypercholesterolemia. To determine the role of ERK5 S496 phosphorylation in SASP, we utilized the IMC technique that performs a qualitative single-cell assessment of SASP in vivo. We found that SASP events were inhibited in MC-like clusters obtained from ERK5 S496A KI plaques, which confirmed the crucial role of ERK5 S496 phosphorylation in SASP induction. More importantly, we found the unique type of MCs, so-called SAS, that escaped from the growth-suppression effects of p53 in the plaque (group 2 in Figure 3A). The induction of SAS was reduced in the plaques from ERK5 S496A KI compared with WT mice. In addition, the increase of SAβ-gal$^+$Ki67$^+$ and 53BP1$^+$Ki67$^+$ macrophages in hypercholesterolemic WT HFD BMDMs compared with those in normocholesterolemic WT NCD BMDMs was attenuated in ERK5 S496A KI mice (Figure 3). These data are in agreement with a critical role of ERK5 S496 phosphorylation in SAS induction. Although senescence in atherosclerotic plaque has been reported,[42] it is challenging to link senescence to plaque formation because of the increase of cell proliferation in the plaque. This paradox is resolved by our demonstration of SAS, which permits macrophages to escape the senescence-induced cell cycle arrest during atherosclerosis formation.

AHR is a ligand-activated transcription factor, which promotes cellular adaptation to environmental changes by sensing compounds from the environment, diet, microbiome, and cellular metabolism.[33] AHR can regulate many biological processes, including angiogenesis, cell motility, and immune modulation. A role for AHR in senescence and atherosclerosis by increasing ROS has been reported.[34,43–47] Since AHR was the most significantly upregulated gene, by hypercholesterolemia-mediated ERK5 S496 phosphorylation in MCs, we examined its role in SAS induction. We found that AHR depletion inhibited the SAS phenotype in BMDMs from hypercholesterolemic WT HFD mice (Figure 4K). We also found that ERK5 S496A and NRF2 K518R mutant inhibited AHR expression and induction of SAS phenotype. Taken together, these data indicate a crucial role of ERK5 S496 phosphorylation and subsequent NRF2 K518 SUMOylation on AHR induction in the initiation of SAS (Figure 7M). Further investigation will be necessary to determine how AHR can regulate SAS phenotype.

Of significance, 2 ERK5 kinase inhibitors (XMD8-92 and a highly selective inhibitor, AX15836) inhibited ERK5 S496 phosphorylation (Figure 5D, 5E, 5H, and 5I; Figure S7C, S7D, S7H, and S7I). There are still conflicting results regarding the functional role of ERK5 catalytic activity. ERK5 contains not only kinase and transcriptional activity but also possesses noncatalytic functions. Therefore, the function of ERK5 may be different depending on which component (kinase, transcriptional activity, and ERK5 S496 phosphorylation-NRF2 K518 SUMOylation) is dominant in the condition under study. For example, Wilhelmsen et al[24,48] reported that the proinflammatory role of ERK5 is induced by proinflammatory cytokines such as IL-1β, TNFα, and Toll-like receptor 2 agonists. However, we[18] and others[49] found that ERK5 has anti-inflammatory effects in the context of shear stress. We found that shear stress increased only ERK5 TEY motif phosphorylation and had no effect on p90RSK and ERK5 S496 phosphorylation.[7] In contrast, cytokines and oxLDL increased p90RSK activation[50] and ERK5 S496 phosphorylation, but the effects on ERK5 TEY motif phosphorylation were minimum (Figure 1A). Therefore, the difference in ERK5 posttranslational modification in response to each stimulus could be the key to explaining these controversies. These data also indicate that not only ERK5 catalytic activity but also ERK5 S496 phosphorylation-NRF2 K518 SUMOylation should be considered when assessing the role of ERK5 in various situations (Figure 7M).

The depletion of NRF2 in bone marrow–derived cells accelerated atherosclerosis formation in LDLR$^{-/-}$ (low density lipoprotein receptor) mice by inducing proinflammatory gene expression.[51] There are several potential mechanisms that induce cross talk between NRF2 and NF-κB signaling. For example, the increase of ROS caused by NRF2 depletion can activate IKK (Inhibitor Of Nuclear Factor Kappa-B Kinase) and increase proinflammatory gene expression.[52] Furthermore, NRF2 could intervene in the senescence process by disrupting proteostasis, altering genomic stability, and causing telomere dysfunction and apoptosis.[53] We and others[54,55] reported a crucial role of NRF2 in upregulating efferocytosis. Previously, we also showed that the NRF2 activator abolished SASP events in BMDMs.[1] In the current study, we found a role for ERK5 S496 phosphorylation in reducing NRF2 transcriptional activity and AHR-SAS induction via upregulation of NRF2 K518 SUMOylation. The role of NRF2 in upregulating CD36 expression has been implicated in the depletion of NRF2-mediated reduction of atherosclerotic plaque formation.[56] We detected that NRF2 K518R inhibited oxLDL-induced CD36

Figure 5 Continued. granulocyte-macrophage colony-stimulating factor (GM-CSF; 20 ng/mL; **B**–**F**), oxidized LDL (low-density lipoprotein; oxLDL; 10 μg/mL; **G**–**K**), or vehicle. Cell lysates were collected after 24 hours of stimulation, and western blotting was performed by the indicated antibodies. Representative images from 5 independent experiments are shown (quantification data were shown in Figure S7). **K**, BMDMs were treated with indicated mutants and inhibitors as described above, and mitochondrial reactive oxygen species (mtROS) production was detected by MitoNeoD as described in the Methods. The applied statistical tests, sample number, and results in all figures are summarized in Table S3. Mean±SD; $^{**}P<0.01$.

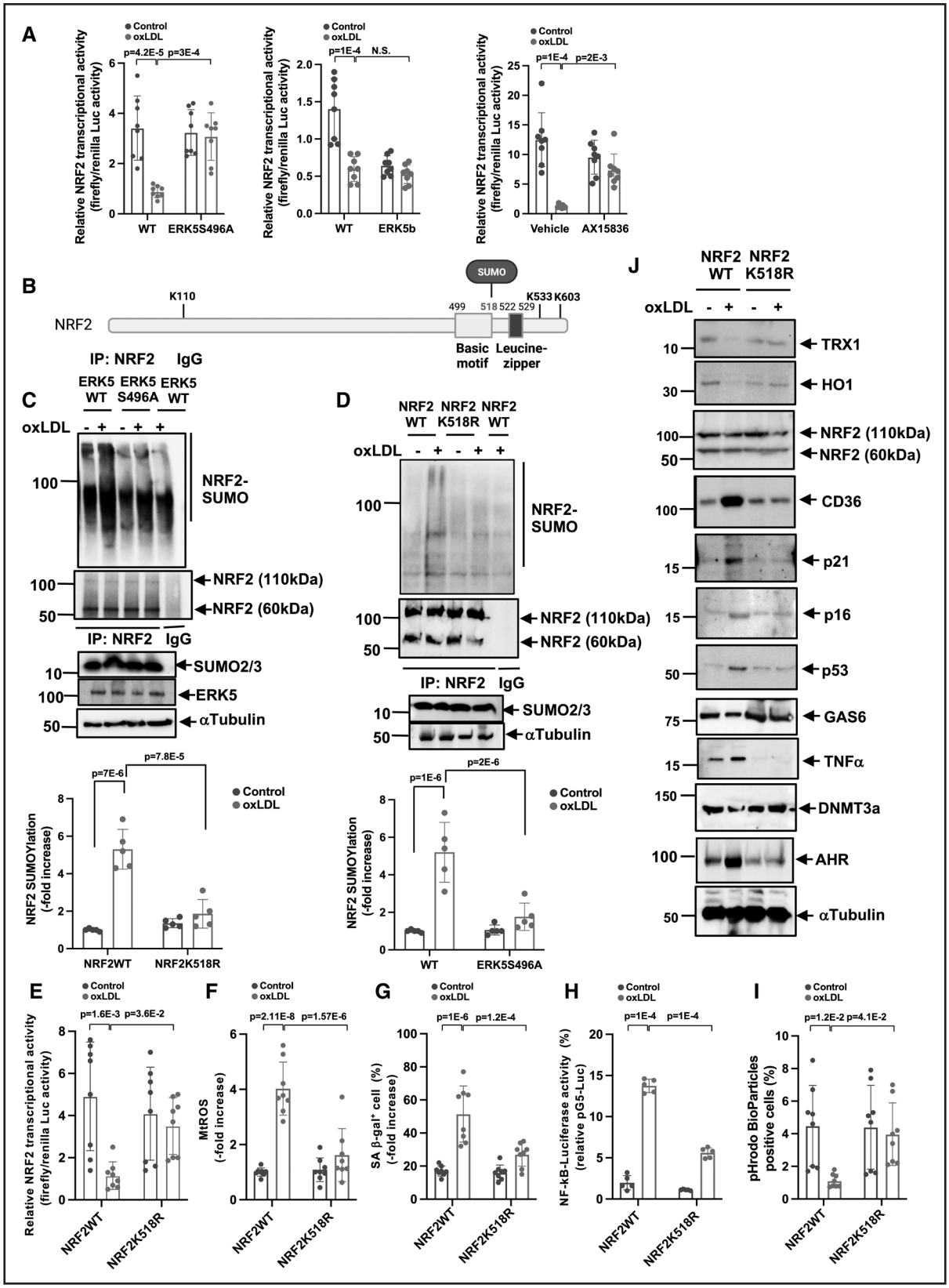

Figure 6. NRF2 (NFE2-related factor 2) K518 SUMOylation mediated by ERK5 (extracellular signal-regulated kinase 5) S496 phosphorylation inhibits NRF2 transcriptional activity and subsequent senescence-associated secretory phenotype (SASP) induction in vitro.

A, Bone marrow–derived macrophages (BMDMs) were transfected with the ERK5 wild type (WT), ERK5 S496A, or ERK5b plasmid and ARE luciferase reporter and the constitutively expressing *Renilla* luciferase vector. After 16 hours of transfection, cells were pretreated (*Continued*)

expression (Figure 6J), which points to different roles for NRF2 depletion and NRF2 K518 SUMOylation in the regulation of CD36 expression. Taken together, these data indicate a critical role of ERK5 S496 phosphorylation–mediated NRF2 SUMOylation in SASP/SAS and consequently accelerated atherosclerosis (Figure 7M).

We found that the mutation of ERK5 S496A inhibited unstable plaque formation and SASP events in MCs in the plaque. However, ERK5 S496 phosphorylation instigated not only SASP but also SAS via upregulating AHR expression. The involvement of senescence in atherosclerosis formation has already been suggested,[57] but the exact molecular mechanisms of senescence-induced atherosclerosis remain unclear. SASP is usually claimed to favor atherosclerosis formation by producing numerous inflammatory cytokines[58] and growth factors[59] that lead to neighboring cells' proliferation.[60,61] To the best of our knowledge, our study provides the first evidence in favor of the hypothesis that the senescent MCs themselves can proliferate by escaping p53-mediated cell cycle arrest and contribute to plaque formation. This is important for understanding the persistent effects of stress-induced senescence, which can be caused by internal and external stimuli such as stress, radiation, and cancer therapy.[62] It is already known that many stressors or stressful events that are transient can have a persistent impact on atherosclerosis formation.[63] If SAS does not take place and senescent cells cannot proliferate, these senescent cells should disappear as they would be removed from the plaque shortly after termination of the transient stress.[64] However, we found evidence for the appearance of SAS in the plaque. Therefore, a transient stress can have long-lasting effects during plaque formation because SAS MCs induced by transient stress can proliferate, thereby maintaining their SASP phenotype. These findings point to the importance of phenotypic changes and reprogramming of MCs in atherosclerosis formation that occurs years after the termination of transient stress such as cancer treatments[62] and sepsis.[63] Further investigation is necessary to clarify this putative mechanism.

We are aware of the fact that our study has several limitations. First, we could not use MC-specific ERK5 S496A KI mice. Therefore, we cannot conclude that the SASP/SAS phenotype observed in this mouse model is uniquely due to MC ERK5 S496 phosphorylation. However, since we could not observe apparent SASP and SAS phenotype in VSMCs and ECs (Figure S2D, S2G through S2K), we can still propose that MC ERK5 S496 phosphorylation plays a critical role in the induction of SASP/SAS phenotype in atherosclerotic plaque. Another limitation is the possible difference in the MC phenotype observed in the plaque and the one occurring in BMDMs.[65] However, our data show that the phenotype of bone marrow cells in HFD mice is quite different from the one observed in NCD mice. Therefore, MC SASP/SAS phenotypic changes already take place in the bone marrow, before entering the vessel wall. To determine the MC phenotype independently of the environmental effects taking place in the plaque, it will be necessary to isolate macrophages from the plaque and check and compare gene expression levels in BMDMs and plaque-derived macrophages. The third limitation is that we do not yet show the real impact on plaque formation of the relatively small number of SAS cells we observed in our conditions (1%–1.5% in the plaque). In the current study, we were able to demonstrate the critical role played by ERK5 S496A phosphorylation and AHR expression in the induction of SAS. However, these events are not specific to SAS induction. Therefore, we still need to develop an appropriate tool to specifically inhibit SAS induction, before being able to ensure that SAS plays an essential role in atherosclerosis. This step is still necessary to investigate the molecular mechanism by which SAS is regulated and to define the pathophysiological role of SAS in plaque formation.

Figure 6 Continued. with AX15836 for 1 hour and then treated with oxidized LDL (low-density lipoprotein; oxLDL; 10 μg/mL) or vehicle. After 12 hours, ARE transcriptional activity was measured as described in Methods. **B**, The scheme of NRF2 SUMOylation sites and DNA-binding sites. **C**, WT BMDMs and ERK5 S496A knock in (KI) BMDMs were incubated with oxLDL or vehicle. After 0 or 30 minutes of oxLDL incubation, cell lysates were immunoprecipitated with anti-NRF2 or IgG control and immunoblotted with SUMO2/3 antibody. **D**, BMDMs were transfected with GFP-tagged NRF2 K518R mutant or GFP tag plasmid. After 0 or 30 minutes of oxLDL incubation, cell lysates were immunoprecipitated with anti-NRF2 or IgG control and immunoblotted with SUMO2/3 antibody. The lower graphs represent densitometry data from 5 independent gels, one of which is shown in **C** and **D**. **E**, WT BMDMs were transfected with NRF K518R mutant or NRF2 WT, the ARE luciferase reporter, and the constitutively expressing *Renilla* luciferase vector for 16 hours. Cells were treated with oxLDL (10 μg/mL) or vehicle, and 6 hours later, NRF2 transcriptional activity was measured as described in Methods. **F**, WT BMDMs were transfected with NRF2 or control siRNA, and after 48 hours of transfection, mitochondrial reactive oxygen species (mtROS) levels were detected by MitoNeoD as described in Methods. Cells treated with oxLDL or vehicle were assayed 12 hours later. **G**, The percentages of cells positive for SA-β-gal (senescence-associated β-gal) staining are shown. More than 200 cells per sample were counted. **H**, NF-κB (nuclear factor kappa B) transcriptional activity was measured as described in Figure 1M in BMDMs transfected with NRF2 K518R mutant or WT after 24 hours of oxLDL or vehicle treatment. **I**, BMDMs were incubated with oxLDL or vehicle after NRF2 K518R mutant or WT transfection. After 24 hours of oxLDL incubation, pHrodo-positive cells were quantified. **J**, BMDMs transfected with NRF2 K518R mutant or WT were treated with oxLDL (10 μg/mL) or vehicle. After 0 to 24 hours, Western blotting was performed with the indicated antibodies. Representative images from 5 independent experiments are shown (quantification was shown in Figure S8C). The applied statistical tests, sample number, and results in all figures are summarized in Table S3. All data are expressed as mean±SD; $^{**}P<0.01$, $^{*}P<0.05$.

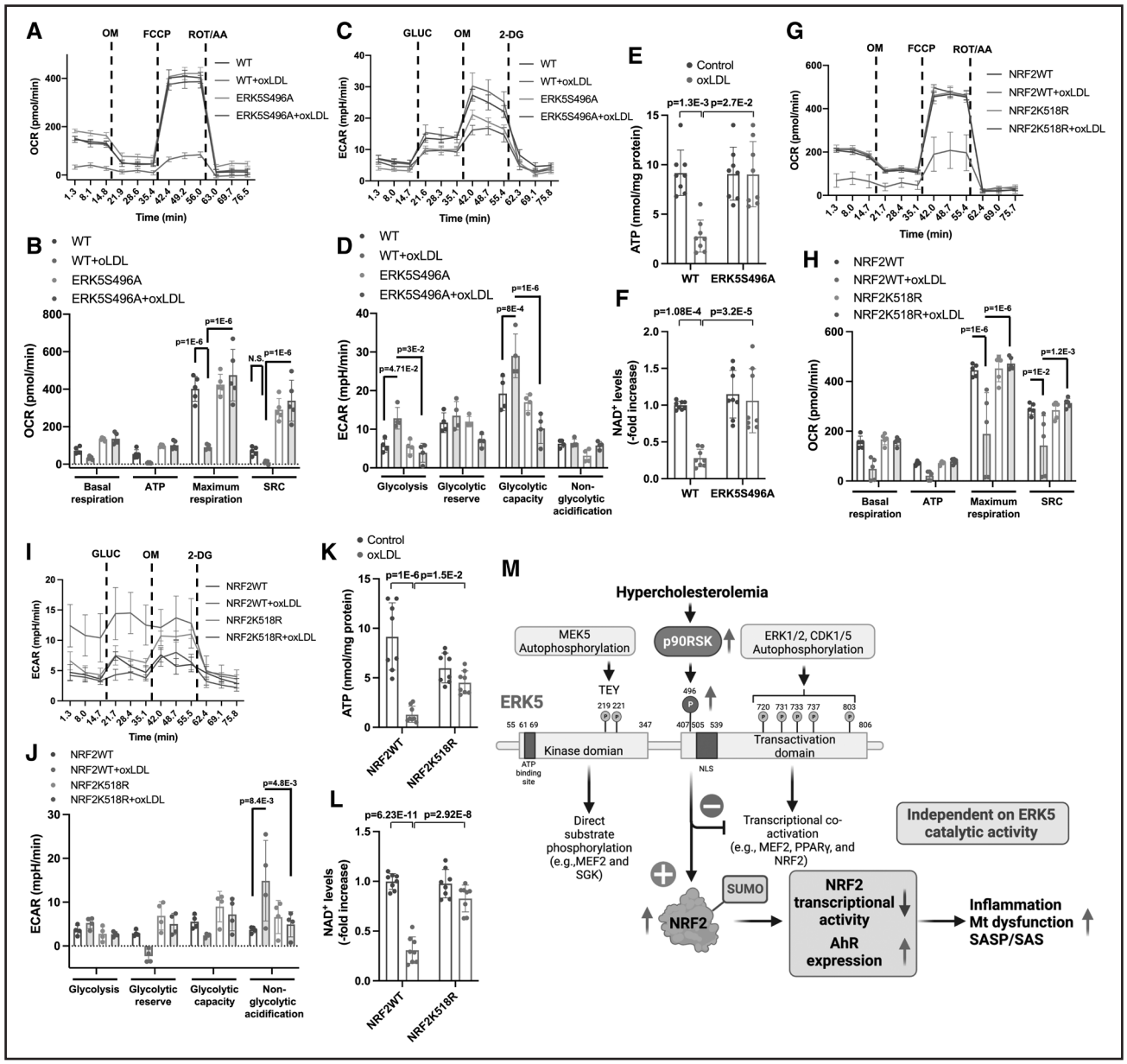

Figure 7. ERK5 (extracellular signal-regulated kinase 5) S496 phosphorylation and NRF2 (NFE2-related factor 2) K518 SUMOylation mediate mitochondrial dysfunction in vitro.

A–**F**, Wild type (WT) bone marrow–derived macrophages (BMDMs) and ERK5 S496A knock in (KI) BMDMs and (**G**–**L**) BMDMs transfected with NRF2 K518R and control plasmid, incubated with oxidized LDL (low-density lipoprotein; oxLDL; 10 μg/mL) or vehicle. These cells were then seeded on Seahorse plates. After 24 hours, oxidative phosphorylation (OXPHOS) and glycolysis parameters were measured. During extracellular flux analysis, cells were sequentially treated with (**A** and **G**) oligomycin (OM), carbonyl cyanide 4-(trifluoromethoxy) phenylhydrazone (FCCP), and rotenone plus antimycin A (ROT/AA) and used to assess OXPHOS parameters based on oxygen consumption rates. **B** and **H**, The basal respiration, mt ATP production, maximal respiration, and spare respiratory capacity were calculated and plotted as oxygen consumption rates in pmoles/min. **C** and **I**, Glucose (GLUC), OM, and 2-deoxyglucose (2-DG) were used to determine glycolysis parameters from extracellular acidification rates. **D** and **J**, Glycolysis, glycolytic reserve, glycolytic capacity, and nonglycolytic acidification were calculated and plotted as the extracellular acidification rate in mpH/min. ATP (**E** and **K**) and NAD^+ (**F** and **L**) were measured after 24 hours of oxLDL (10 μg/mL) or vehicle treatment in WT BMDMs and ERK5 S496A KI BMDMs. **M**, Proposed model of HC-mediated MC reprogramming to senescence-associated secretory phenotype (SASP)/senescence-associated stemness (SAS) by ERK5 S496 phosphorylation. The applied statistical tests, sample number, and results in all figures are summarized in Table S3. All data except **A**, **C**, **G**, and **I** are expressed as mean±SD, and others are expressed as mean±SEM; $^{**}P<0.01$, $^{*}P<0.05$.

ARTICLE INFORMATION

Received September 20, 2022; revision received May 9, 2023; accepted May 17, 2023.

Affiliations

Departments of Cardiology (J.-i.A., M.I., K.A.K., V.S.K.S., L.-L.L., A.P.B., Y.J.G., A.D., N.L.P., K.F., S. Kotla), Radiation Oncology (S.H.L.), Pediatric Research (K.L.S.), Emergency Medicine (C.R.-G., S.-C.J.Y.), Symptom Research (R.D.), and Leukemia, Division of Cancer Medicine (J.K.B.), The University of Texas MD Anderson Cancer Center, Houston, TX. Department of Cardiovascular Sciences (S.L., T.-H.-M.N., R.J.A., E.A.O.-D., J.P.C., G.W., N.-T.L.) and Center for Bioenergetics (A.Z., A.A.G., H.J.P., D.J.H.), Houston Methodist Research Institute, Houston, TX. Department of Medicine, Houston Methodist, Weill Cornell Medicine Affiliate, Houston, TX (A.Z., A.A.G., H.J.P., D.J.H.). Department of Population Health, The University of Texas at Austin, Austin, TX (B.P.H.). Cardio Oncology Clinic, Division of Preventive Cardiology, Department of Cardiovascular Medicine, Mayo Clinic, Rochester, MN (J.H.). Department of Anesthesiology and Perioperative Medicine, Mayo Clinic, Jacksonville, FL (E.N.C.). Division of Cardiothoracic Surgery, Baylor College of Medicine, Houston, TX (Y.H.S.). Department of Neurosurgery (S. Krishnan) and Center for Stem Cell and Regenerative Medicine, Institute of Molecular Medicine (M.Y.), The University of Texas Health Science Center at Houston, Houston, TX.

Acknowledgments

We thank Scientific Publications, Research Medical Library at The University of Texas MD Anderson Cancer Center for editing, Carolyn J. Giancursio for her technical assistance, and Darrel R. Schroeder for helping statistical analysis.

Author Contributions

M. Imanishi performed the experiments, interpreted the data, and wrote the manuscript. S. Li, A. Zhang, and K.A. Ko performed the experiments and analyzed the data. A.A. Gupte supported data analyses. V.S.K. Samanthapudi, A.P. Bojorges, and Y.J. Gi maintained mouse colonies. K.L. Schadler, A. Deswal, J. Herrmann, S.H. Lin, E.N. Chini, Y.H. Shen, R.J. Abe, T.-H.-M. Nguyen, C. Reyes-Gibby, S.-C.J. Yeung, E.A. Olmsted-Davis, R. Dantzer, N.L. Palaskas, J.P. Cooke, S. Krishnan, H.J. Pownall, and K. Fujiwara contributed to the interpretation of the data. J.K. Burks planned and analyzed imaging mass cytometry data. B.P. Hobbs supported the statistical analyses. N.-T. Le, D.J. Hamilton, G. Wang, and J.-i. Abe planned and generated the study design, obtained funding, interpreted data, and wrote the manuscript. S. Kolta performed the experiments, interpreted the data, planned and generated the study design, obtained funding, interpreted data, and wrote the manuscript.

Sources of Funding

This work was partially supported by grants from the National Institutes of Health to J.-i. Abe (HL-149303 and AI-156921), J.P. Cooke (HL-149303), and N.-T. Le (HL-134740 and HL-149303) and from the Cancer Prevention and Research Institute of Texas (CPRIT) to J.-i. Abe and K.L. Schadler (RP190256). This work is also partially supported by the University of Texas MD Anderson Cancer Center Institutional Research Grant Program to S. Kotla. This research was performed in the Flow Cytometry and Cellular Imaging Core Facility, which is supported, in part, by the National Institutes of Health through MD Anderson's Cancer Center Support Grant CA016672, the NCI's Research Specialist 1 R50 CA243707-01A1, and a Shared Instrumentation Award from CPRIT, RP121010.

Disclosures

S.H. Lin is an Advisory Board member of AstraZeneca, Beyond Spring Pharmaceuticals, and STCube Pharmaceuticals. The other authors report no conflicts.

Supplemental Material

Supplemental Methods
Contact for Reagent and Resource Sharing
Experimental Model and Subject Details
Methods Details
Supplemental Discussion
Figures S1–S8
Tables S1–S5
Major Resources Table
Raw Data Sets: Files S1–S3
References 66–95

REFERENCES

1. Singh MV, Kotla S, Le NT, Ae Ko K, Heo KS, Wang Y, Fujii Y, Thi Vu H, McBeath E, Thomas TN, et al. Senescent phenotype induced by p90RSK-NRF2 signaling sensitizes monocytes and macrophages to oxidative stress in HIV-positive individuals. *Circulation*. 2019;139:1199–1216. doi: 10.1161/CIRCULATIONAHA.118.036232
2. Kitada M, Ogura Y, Koya D. The protective role of Sirt1 in vascular tissue: its relationship to vascular aging and atherosclerosis. *Aging (Albany NY)*. 2016;8:2290–2307. doi: 10.18632/aging.101068
3. Du W, Wong C, Song Y, Shen H, Mori D, Rotllan N, Price N, Dobrian AD, Meng H, Kleinstein SH, et al. Age-associated vascular inflammation promotes monocytosis during atherogenesis. *Aging Cell*. 2016;15:766–777. doi: 10.1111/acel.12488
4. Wang JC, Bennett M. Aging and atherosclerosis: mechanisms, functional consequences, and potential therapeutics for cellular senescence. *Circ Res*. 2012;111:245–259. doi: 10.1161/CIRCRESAHA.111.261388
5. Li W. Phagocyte dysfunction, tissue aging and degeneration. *Ageing Res Rev*. 2013;12:1005–1012. doi: 10.1016/j.arr.2013.05.006
6. Niccoli T, Partridge L. Ageing as a risk factor for disease. *Curr Biol*. 2012;22:R741–R752. doi: 10.1016/j.cub.2012.07.024
7. Le NT, Heo KS, Takei Y, Lee H, Woo CH, Chang E, McClain C, Hurley C, Wang X, Li F, et al. A crucial role for p90RSK-mediated reduction of ERK5 transcriptional activity in endothelial dysfunction and atherosclerosis. *Circulation*. 2013;127:486–499. doi: 10.1161/CIRCULATIONAHA.112.116988
8. Faget DV, Ren Q, Stewart SA. Unmasking senescence: context-dependent effects of SASP in cancer. *Nat Rev Cancer*. 2019;19:439–453. doi: 10.1038/s41568-019-0156-2
9. Milanovic M, Yu Y, Schmitt CA. The senescence-stemness alliance - a cancer-hijacked regeneration principle. *Trends Cell Biol*. 2018;28:1049–1061. doi: 10.1016/j.tcb.2018.09.001
10. Milanovic M, Fan DNY, Belenki D, Dabritz JHM, Zhao Z, Yu Y, Dorr JR, Dimitrova L, Lenze D, Monteiro Barbosa IA, et al. Senescence-associated reprogramming promotes cancer stemness. *Nature*. 2018;553:96–100. doi: 10.1038/nature25167
11. Dou Z, Berger SL. Senescence elicits stemness: a surprising mechanism for cancer relapse. *Cell Metab*. 2018;27:710–711. doi: 10.1016/j.cmet.2018.03.009
12. Coppe JP, Rodier F, Patil CK, Freund A, Desprez PY, Campisi J. Tumor suppressor and aging biomarker p16(INK4a) induces cellular senescence without the associated inflammatory secretory phenotype. *J Biol Chem*. 2011;286:36396–36403. doi: 10.1074/jbc.M111.257071
13. Ferrand M, Kirsh O, Griveau A, Vindrieux D, Martin N, Defossez PA, Bernard D. Screening of a kinase library reveals novel pro-senescence kinases and their common NF-kappaB-dependent transcriptional program. *Aging (Albany NY)*. 2015;7:986–1003. doi: 10.18632/aging.100845
14. Saleh T, Tyutynuk-Massey L, Cudjoe EK Jr, Idowu MO, Landry JW, Gewirtz DA. Non-cell autonomous effects of the senescence-associated secretory phenotype in cancer therapy. *Front Oncol*. 2018;8:164. doi: 10.3389/fonc.2018.00164
15. Saleh T, Tyutyunyk-Massey L, Murray GF, Alotaibi MR, Kawale AS, Elsayed Z, Henderson SC, Yakovlev V, Elmore LW, Toor A, et al. Tumor cell escape from therapy-induced senescence. *Biochem Pharmacol*. 2019;162:202–212. doi: 10.1016/j.bcp.2018.12.013
16. Munoz DP, Yannone SM, Daemen A, Sun Y, Vakar-Lopez F, Kawahara M, Freund AM, Rodier F, Wu JD, Desprez PY, et al. Targetable mechanisms driving immunoevasion of persistent senescent cells link chemotherapy-resistant cancer to aging. *JCI Insight*. 2019;5:e124716. doi: 10.1172/jci.insight.124716
17. Tang J, Lobatto ME, Hassing L, van der Staay S, van Rijs SM, Calcagno C, Braza MS, Baxter S, Fay F, Sanchez-Gaytan BL, et al. Inhibiting macrophage proliferation suppresses atherosclerotic plaque inflammation. *Sci Adv*. 2015;1:e1400223. doi: 10.1126/sciadv.1400223
18. Akaike M, Che W, Marmarosh NL, Ohta S, Osawa M, Ding B, Berk BC, Yan C, Abe J. The hinge-helix 1 region of peroxisome proliferator-activated receptor gamma1 (PPARgamma1) mediates interaction with extracellular signal-regulated kinase 5 and PPARgamma1 transcriptional activation: involvement in flow-induced PPARgamma activation in endothelial cells. *Mol Cell Biol*. 2004;24:8691–8704. doi: 10.1128/MCB.24.19.8691-8704.2004
19. Kasler HG, Victoria J, Duramad O, Winoto A. ERK5 is a novel type of mitogen-activated protein kinase containing a transcriptional activation domain. *Mol Cell Biol*. 2000;20:8382–8389. doi: 10.1128/MCB.20.22.8382-8389.2000

20. Kato Y, Kravchenko VV, Tapping RI, Han J, Ulevitch RJ, Lee JD. BMK1/ERK5 regulates serum-induced early gene expression through transcription factor MEF2C. *EMBO J.* 1997;16:7054–7066. doi: 10.1093/emboj/16.23.7054
21. Kim M, Kim S, Lim JH, Lee C, Choi HC, Woo CH. Laminar flow activation of ERK5 protein in vascular endothelium leads to atheroprotective effect via NF-E2-related factor 2 (Nrf2) activation. *J Biol Chem.* 2012;287:40722–40731. doi: 10.1074/jbc.M112.381509
22. Pearson G, English JM, White MA, Cobb MH. ERK5 and ERK2 cooperate to regulate NF-kappaB and cell transformation. *J Biol Chem.* 2001;276:7927–7931. doi: 10.1074/jbc.M009764200
23. Maciejczyk M, Mikoluc B, Pietrucha B, Heropolitanska-Pliszka E, Pac M, Motkowski R, Car H. Oxidative stress, mitochondrial abnormalities and antioxidant defense in Ataxia-telangiectasia, Bloom syndrome and Nijmegen breakage syndrome. *Redox Biol.* 2017;11:375–383. doi: 10.1016/j.redox.2016.12.030
24. Wilhelmsen K, Xu F, Farrar K, Tran A, Khakpour S, Sundar S, Prakash A, Wang J, Gray NS, Hellman J. Extracellular signal-regulated kinase 5 promotes acute cellular and systemic inflammation. *Sci Signal.* 2015;8:ra86. doi: 10.1126/scisignal.aaa3206
25. Lin EC, Amantea CM, Nomanbhoy TK, Weissig H, Ishiyama J, Hu Y, Sidique S, Li B, Kozarich JW, Rosenblum JS. ERK5 kinase activity is dispensable for cellular immune response and proliferation. *Proc Natl Acad Sci USA.* 2016;113:11865–11870. doi: 10.1073/pnas.1609019113
26. Lochhead PA, Tucker JA, Tatum NJ, Wang J, Oxley D, Kidger AM, Johnson VP, Cassidy MA, Gray NS, Noble MEM, et al. Paradoxical activation of the protein kinase-transcription factor ERK5 by ERK5 kinase inhibitors. *Nat Commun.* 2020;11:1383. doi: 10.1038/s41467-020-15031-3
27. Kotla S, Zhang A, Imanishi M, Ko KA, Lin SH, Gi YJ, Moczygemba M, Isgandarova S, Schadler KL, Chung C, et al. Nucleus-mitochondria positive feedback loop formed by ERK5 S496 phosphorylation-mediated poly (ADP-ribose) polymerase activation provokes persistent pro-inflammatory senescent phenotype and accelerates coronary atherosclerosis after chemoradiation. *Redox Biol.* 2021;47:102132. doi: 10.1016/j.redox.2021.102132
28. Schieffer B, Selle T, Hilfiker A, Hilfiker-Kleiner D, Grote K, Tietge UJ, Trautwein C, Luchtefeld M, Schmittkamp C, Heeneman S, et al. Impact of interleukin-6 on plaque development and morphology in experimental atherosclerosis. *Circulation.* 2004;110:3493–3500. doi: 10.1161/01.CIR.0000148135.08582.97
29. Herranz N, Gil J. Mechanisms and functions of cellular senescence. *J Clin Invest.* 2018;128:1238–1246. doi: 10.1172/JCI95148
30. Merched AJ, Williams E, Chan L. Macrophage-specific p53 expression plays a crucial role in atherosclerosis development and plaque remodeling. *Arterioscler Thromb Vasc Biol.* 2003;23:1608–1614. doi: 10.1161/01.ATV.0000084825.88022.53
31. Sinha SK, Miikeda A, Fouladian Z, Mehrabian M, Edillor C, Shih D, Zhou Z, Paul MK, Charugundla S, Davis RC, et al. Local M-CSF (macrophage colony-stimulating factor) expression regulates macrophage proliferation and apoptosis in atherosclerosis. *Arterioscler Thromb Vasc Biol.* 2021;41:220–233. doi: 10.1161/ATVBAHA.120.315255
32. Vizioli MG, Liu T, Miller KN, Robertson NA, Gilroy K, Lagnado AB, Perez-Garcia A, Kiourtis C, Dasgupta N, Lei X, et al. Mitochondria-to-nucleus retrograde signaling drives formation of cytoplasmic chromatin and inflammation in senescence. *Genes Dev.* 2020;34:428–445. doi: 10.1101/gad.331272.119
33. Feng S, Cao Z, Wang X. Role of aryl hydrocarbon receptor in cancer. *Biochim Biophys Acta.* 2013;1836:197–210. doi: 10.1016/j.bbcan.2013.05.001
34. Kaiser H, Parker E, Hamrick MW. Kynurenine signaling through the aryl hydrocarbon receptor: implications for aging and healthspan. *Exp Gerontol.* 2020;130:110797. doi: 10.1016/j.exger.2019.110797
35. Yan C, Luo H, Lee JD, Abe J, Berk BC. Molecular cloning of mouse ERK5/BMK1 splice variants and characterization of ERK5 functional domains. *J Biol Chem.* 2001;276:10870–10878. doi: 10.1074/jbc.M009286200
36. Kato Y, Tapping RI, Huang S, Watson MH, Ulevitch RJ, Lee JD. Bmk1/Erk5 is required for cell proliferation induced by epidermal growth factor. *Nature.* 1998;395:713–716. doi: 10.1038/27234
37. Le NT, Takei Y, Shishido T, Woo CH, Chang E, Heo KS, Lee H, Lu Y, Morrell C, Oikawa M, et al. p90RSK targets the ERK5-CHIP ubiquitin E3 ligase activity in diabetic hearts and promotes cardiac apoptosis and dysfunction. *Circ Res.* 2012;110:536–550. doi: 10.1161/CIRCRESAHA.111.254730
38. Abe JI, Sandhu UG, Hoang NM, Thangam M, Quintana-Quezada RA, Fujiwara K, Le NT. Coordination of cellular localization-dependent effects of sumoylation in regulating cardiovascular and neurological diseases. *Adv Exp Med Biol.* 2017;963:337–358. doi: 10.1007/978-3-319-50044-7_20
39. He X, Lai Q, Chen C, Li N, Sun F, Huang W, Zhang S, Yu Q, Yang P, Xiong F, et al. Both conditional ablation and overexpression of E2 SUMO-conjugating enzyme (UBC9) in mouse pancreatic beta cells result in impaired beta cell function. *Diabetologia.* 2018;61:881–895. doi: 10.1007/s00125-017-4523-9
40. Guo H, Xu J, Zheng Q, He J, Zhou W, Wang K, Huang X, Fan Q, Ma J, Cheng J, et al. NRF2 SUMOylation promotes de novo serine synthesis and maintains HCC tumorigenesis. *Cancer Lett.* 2019;466:39–48. doi: 10.1016/j.canlet.2019.09.010
41. Hendriks IA, D'Souza RC, Yang B, Verlaan-de Vries M, Mann M, Vertegaal AC. Uncovering global SUMOylation signaling networks in a site-specific manner. *Nat Struct Mol Biol.* 2014;21:927–936. doi: 10.1038/nsmb.2890
42. Dominic A, Banerjee P, Hamilton DJ, Le NT, Abe JI. Time-dependent replicative senescence vs. disturbed flow-induced premature aging in atherosclerosis. *Redox Biol.* 2020;37:101614. doi: 10.1016/j.redox.2020.101614
43. Hu P, Herrmann R, Bednar A, Saloupis P, Dwyer MA, Yang P, Qi X, Thomas RS, Jaffe GJ, Boulton ME, et al. Aryl hydrocarbon receptor deficiency causes dysregulated cellular matrix metabolism and age-related macular degeneration-like pathology. *Proc Natl Acad Sci USA.* 2013;110:E4069–E4078. doi: 10.1073/pnas.1307574110
44. Eckers A, Jakob S, Heiss C, Haarmann-Stemmann T, Goy C, Brinkmann V, Cortese-Krott MM, Sansone R, Esser C, Ale-Agha N, et al. The aryl hydrocarbon receptor promotes aging phenotypes across species. *Sci Rep.* 2016;6:19618. doi: 10.1038/srep19618
45. Bravo-Ferrer I, Cuartero MI, Medina V, Ahedo-Quero D, Pena-Martinez C, Perez-Ruiz A, Fernandez-Valle ME, Hernandez-Sanchez C, Fernandez-Salguero PM, Lizasoain I, et al. Lack of the aryl hydrocarbon receptor accelerates aging in mice. *FASEB J.* 2019;33:12644–12654. doi: 10.1096/fj.201901333R
46. Brinkmann V, Ale-Agha N, Haendeler J, Ventura N. The Aryl hydrocarbon receptor (AhR) in the aging process: another puzzling role for this highly conserved transcription factor. *Front Physiol.* 2019;10:1561. doi: 10.3389/fphys.2019.01561
47. Kerley-Hamilton JS, Trask HW, Ridley CJ, Dufour E, Lesseur C, Ringelberg CS, Moodie KL, Shipman SL, Korc M, Gui J, et al. Inherent and benzo[a]pyrene-induced differential aryl hydrocarbon receptor signaling greatly affects life span, atherosclerosis, cardiac gene expression, and body and heart growth in mice. *Toxicol Sci.* 2012;126:391–404. doi: 10.1093/toxsci/kfs002
48. Wilhelmsen K, Mesa KR, Lucero J, Xu F, Hellman J. ERK5 protein promotes, whereas MEK1 protein differentially regulates, the Toll-like receptor 2 protein-dependent activation of human endothelial cells and monocytes. *J Biol Chem.* 2012;287:26478–26494. doi: 10.1074/jbc.M112.359489
49. Parmar KM, Larman HB, Dai G, Zhang Y, Wang ET, Moorthy SN, Kratz JR, Lin Z, Jain MK, Gimbrone MA Jr, et al. Integration of flow-dependent endothelial phenotypes by Kruppel-like factor 2. *J Clin Invest.* 2006;116:49–58. doi: 10.1172/JCI24787
50. Peng C, Cho YY, Zhu F, Xu YM, Wen W, Ma WY, Bode AM, Dong Z. RSK2 mediates NF-{kappa}B activity through the phosphorylation of IkappaBalpha in the TNF-R1 pathway. *FASEB J.* 2010;24:3490–3499. doi: 10.1096/fj.09-151290
51. Ruotsalainen AK, Inkala M, Partanen ME, Lappalainen JP, Kansanen E, Makinen PI, Heinonen SE, Laitinen HM, Heikkila J, Vatanen T, et al. The absence of macrophage Nrf2 promotes early atherogenesis. *Cardiovasc Res.* 2013;98:107–115. doi: 10.1093/cvr/cvt008
52. Nakajima S, Kitamura M. Bidirectional regulation of NF-kappaB by reactive oxygen species: a role of unfolded protein response. *Free Radic Biol Med.* 2013;65:162–174. doi: 10.1016/j.freeradbiomed.2013.06.020
53. Tsakiri EN, Sykiotis GP, Papassideri IS, Terpos E, Dimopoulos MA, Gorgoulis VG, Bohmann D, Trougakos IP. Proteasome dysfunction in Drosophila signals to an Nrf2-dependent regulatory circuit aiming to restore proteostasis and prevent premature aging. *Aging Cell.* 2013;12:802–813. doi: 10.1111/acel.12111
54. Kim W, Kim HU, Lee HN, Kim SH, Kim C, Cha YN, Joe Y, Chung HT, Jang J, Kim K, et al. Taurine chloramine stimulates efferocytosis through upregulation of Nrf2-mediated heme oxygenase-1 expression in murine macrophages: possible involvement of carbon monoxide. *Antioxid Redox Signal.* 2015;23:163–177. doi: 10.1089/ars.2013.5825
55. Helou DG, Noel B, Gaudin F, Groux H, El Ali Z, Pallardy M, Chollet-Martin S, Kerdine-Romer S. Cutting edge: Nrf2 regulates neutrophil recruitment and accumulation in skin during contact hypersensitivity. *J Immunol.* 2019;202:2189–2194. doi: 10.4049/jimmunol.1801065
56. Sussan TE, Jun J, Thimmulappa R, Bedja D, Antero M, Gabrielson KL, Polotsky VY, Biswal S. Disruption of Nrf2, a key inducer of antioxidant defenses, attenuates ApoE-mediated atherosclerosis in mice. *PLoS One.* 2008;3:e3791. doi: 10.1371/journal.pone.0003791

57. Dominic A, Banerjee P, Hamilton DJ, Le NT, Abe JI. Time-dependent replicative senescence vs. disturbed flow-induced pre-mature aging in atherosclerosis. *Redox Biol*. 2020;37:101614. doi: 10.1016/j.redox.2020.101614
58. Davalos AR, Coppe JP, Campisi J, Desprez PY. Senescent cells as a source of inflammatory factors for tumor progression. *Cancer Metastasis Rev*. 2010;29:273–283. doi: 10.1007/s10555-010-9220-9
59. Coppe JP, Kauser K, Campisi J, Beausejour CM. Secretion of vascular endothelial growth factor by primary human fibroblasts at senescence. *J Biol Chem*. 2006;281:29568–29574. doi: 10.1074/jbc.M603307200
60. Coppe JP, Patil CK, Rodier F, Sun Y, Munoz DP, Goldstein J, Nelson PS, Desprez PY, Campisi J. Senescence-associated secretory phenotypes reveal cell-nonautonomous functions of oncogenic RAS and the p53 tumor suppressor. *PLoS Biol*. 2008;6:2853–2868. doi: 10.1371/journal.pbio.0060301
61. Ohanna M, Giuliano S, Bonet C, Imbert V, Hofman V, Zangari J, Bille K, Robert C, Bressac-de Paillerets B, Hofman P, et al. Senescent cells develop a PARP-1 and nuclear factor-{kappa}B-associated secretome (PNAS). *Genes Dev*. 2011;25:1245–1261. doi: 10.1101/gad.625811
62. Banerjee P, Kotla S, Reddy Velatooru L, Abe RJ, Davis EA, Cooke JP, Schadler K, Deswal A, Herrmann J, Lin SH, et al. Senescence-associated secretory phenotype as a hinge between cardiovascular diseases and cancer. *Front Cardiovasc Med*. 2021;8:763930. doi: 10.3389/fcvm.2021.763930
63. Merdji H, Schini-Kerth V, Meziani F, Toti F. Long-term cardiovascular complications following sepsis: is senescence the missing link? *Ann Intensive Care*. 2021;11:166. doi: 10.1186/s13613-021-00937-y
64. Sadhu S, Decker C, Sansbury BE, Marinello M, Seyfried A, Howard J, Mori M, Hosseini Z, Arunachalam T, Finn AV, et al. Radiation-induced macrophage senescence impairs resolution programs and drives cardiovascular inflammation. *J Immunol*. 2021;207:1812–1823. doi: 10.4049/jimmunol.2100284
65. Iwata H, Manabe I, Nagai R. Lineage of bone marrow-derived cells in atherosclerosis. *Circ Res*. 2013;112:1634–1647. doi: 10.1161/CIRCRESAHA.113.301384
66. McBeath E, Parker-Thornburg J, Fujii Y, Aryal N, Smith C, Hofmann MC, Abe JI, Fujiwara K. Rapid evaluation of CRISPR guides and donors for engineering mice. *Genes (Basel)*. 2020;11:628. doi: 10.3390/genes11060628
67. Ko KA, Wang Y, Kotla S, Fujii Y, Vu HT, Venkatesulu BP, Thomas TN, Medina JL, Gi YJ, Hada M, et al. Developing a reliable mouse model for cancer therapy-induced cardiovascular toxicity in cancer patients and survivors. *Front Cardiovasc Med*. 2018;5:26. doi: 10.3389/fcvm.2018.00026
68. Knight WE, Chen S, Zhang Y, Oikawa M, Wu M, Zhou Q, Miller CL, Cai Y, Mickelsen DM, Moravec C, et al. PDE1C deficiency antagonizes pathological cardiac remodeling and dysfunction. *Proc Natl Acad Sci USA*. 2016;113:E7116–E7125. doi: 10.1073/pnas.1607728113
69. Gao S, Ho D, Vatner DE, Vatner SF. Echocardiography in mice. *Curr Protoc Mouse Biol*. 2011;1:71–83. doi: 10.1002/9780470942390.mo100130
70. Bjorklund MM, Hollensen AK, Hagensen MK, Dagnaes-Hansen F, Christoffersen C, Mikkelsen JG, Bentzon JF. Induction of atherosclerosis in mice and hamsters without germline genetic engineering. *Circ Res*. 2014;114:1684–1689. doi: 10.1161/CIRCRESAHA.114.302937
71. Thorp E, Li G, Seimon TA, Kuriakose G, Ron D, Tabas I. Reduced apoptosis and plaque necrosis in advanced atherosclerotic lesions of Apoe-/- and Ldlr-/- mice lacking CHOP. *Cell Metab*. 2009;9:474–481. doi: 10.1016/j.cmet.2009.03.003
72. Ren JL, Chen Y, Zhang LS, Zhang YR, Liu SM, Yu YR, Jia MZ, Tang CS, Qi YF, Lu WW. Intermedin(1-53) attenuates atherosclerotic plaque vulnerability by inhibiting CHOP-mediated apoptosis and inflammasome in macrophages. *Cell death & disease*. 2021;12:436. doi: 10.1038/s41419-021-03712-w
73. Venegas-Pino DE, Banko N, Khan MI, Shi Y, Werstuck GH. Quantitative analysis and characterization of atherosclerotic lesions in the murine aortic sinus. *J Vis Exp*. 2013;82:50933. doi: 10.3791/50933
74. Englen MD, Valdez YE, Lehnert NM, Lehnert BE. Granulocyte/macrophage colony-stimulating factor is expressed and secreted in cultures of murine L929 cells. *J Immunol Methods*. 1995;184:281–283. doi: 10.1016/0022-1759(95)00136-x
75. Heo KS, Chang E, Le NT, Cushman H, Yeh ET, Fujiwara K, Abe J. De-SUMOylation enzyme of sentrin/SUMO-specific protease 2 regulates disturbed flow-induced SUMOylation of ERK5 and p53 that leads to endothelial dysfunction and atherosclerosis. *Circ Res*. 2013;112:911–923. doi: 10.1161/CIRCRESAHA.111.300179
76. Wong ML, Medrano JF. Real-time PCR for mRNA quantitation. *Biotechniques*. 2005;39:75–85. doi: 10.2144/05391RV01
77. Shchepinova MM, Cairns AG, Prime TA, Logan A, James AM, Hall AR, Vidoni S, Arndt S, Caldwell ST, Prag HA, et al. MitoNeoD: a mitochondria-targeted superoxide probe. *Cell Chem Biol*. 2017;24:1285–1298.e12. doi: 10.1016/j.chembiol.2017.08.003
78. Bornfeldt KE, Raines EW, Nakano T, Graves LM, Krebs EG, Ross R. Insulin-like growth factor-I and platelet-derived growth factor-BB induce directed migration of human arterial smooth muscle cells via signaling pathways that are distinct from those of proliferation. *J Clin Invest*. 1994;93:1266–1274. doi: 10.1172/JCI117081
79. Heo KS, Cushman HJ, Akaike M, Woo CH, Wang X, Qiu X, Fujiwara K, Abe J. ERK5 activation in macrophages promotes efferocytosis and inhibits atherosclerosis. *Circulation*. 2014;130:180–191. doi: 10.1161/CIRCULATIONAHA.113.005991
80. Debacq-Chainiaux F, Erusalimsky JD, Campisi J, Toussaint O. Protocols to detect senescence-associated beta-galactosidase (SA-betagal) activity, a biomarker of senescent cells in culture and in vivo. *Nat Protoc*. 2009;4:1798–1806. doi: 10.1038/nprot.2009.191
81. Sousa LG, McGrail DJ, Li K, Marques-Piubelli ML, Gonzalez C, Dai H, Ferri-Borgogno S, Godoy M, Burks J, Lin SY, et al. Spontaneous tumor regression following COVID-19 vaccination. *J ImmunoTher Cancer*. 2022;10:e004371. doi: 10.1136/jitc-2021-004371
82. Vidgen B, Yasseri T. P-values: misubnderstood and misused. *Front Phys*. 2016;4:1–5. doi: 10.3389/fphy.2016.00006
83. Fay MP, Proschan MA. Wilcoxon-Mann-Whitney or t-test? On assumptions for hypothesis tests and multiple interpretations of decision rules. *Stat Surv*. 2010;4:1–39. doi: 10.1214/09-SS051
84. Degasperi A, Birtwistle MR, Volinsky N, Rauch J, Kolch W, Kholodenko BN. Evaluating strategies to normalise biological replicates of western blot data. *PLoS One*. 2014;9:e87293. doi: 10.1371/journal.pone.0087293
85. Ortega N, Fanelli A, Serrano A, Martinez-Carrasco C, Escribano F, Tizzani P, Candela MG. Salmonella seroprevalence in wild boar from Southeast Spain depends on host population density. *Res Vet Sci*. 2020;132:400–403. doi: 10.1016/j.rvsc.2020.07.026
86. Krzywinski M, Altman N, Blainey P. Points of significance: nested designs. For studies with hierarchical noise sources, use a nested analysis of variance approach. *Nat Methods*. 2014;11:977–978. doi: 10.1038/nmeth.3137
87. Sharpless NE, Sherr CJ. Forging a signature of in vivo senescence. *Nat Rev Cancer*. 2015;15:397–408. doi: 10.1038/nrc3960
88. Swirski FK, Pittet MJ, Kircher MF, Aikawa E, Jaffer FA, Libby P, Weissleder R. Monocyte accumulation in mouse atherogenesis is progressive and proportional to extent of disease. *Proc Natl Acad Sci USA*. 2006;103:10340–10345. doi: 10.1073/pnas.0604260103
89. Jongstra-Bilen J, Haidari M, Zhu SN, Chen M, Guha D, Cybulsky MI. Low-grade chronic inflammation in regions of the normal mouse arterial intima predisposed to atherosclerosis. *J Exp Med*. 2006;203:2073–2083. doi: 10.1084/jem.20060245
90. Swirski FK, Libby P, Aikawa E, Alcaide P, Luscinskas FW, Weissleder R, Pittet MJ. Ly-6Chi monocytes dominate hypercholesterolemia-associated monocytosis and give rise to macrophages in atheromata. *J Clin Invest*. 2007;117:195–205. doi: 10.1172/JCI29950
91. Cudejko C, Wouters K, Fuentes L, Hannou SA, Paquet C, Bantubungi K, Bouchaert E, Vanhoutte J, Fleury S, Remy P, et al. p16INK4a deficiency promotes IL-4-induced polarization and inhibits proinflammatory signaling in macrophages. *Blood*. 2011;118:2556–2566. doi: 10.1182/blood-2010-10-313106
92. Liu JY, Souroullas GP, Diekman BO, Krishnamurthy J, Hall BM, Sorrentino JA, Parker JS, Sessions GA, Gudkov AV, Sharpless NE. Cells exhibiting strong p16(INK4a) promoter activation in vivo display features of senescence. *Proc Natl Acad Sci U S A*. 2019;116:2603–2611. doi: 10.1073/pnas.1818313116
93. Aguilar G, Cordova F, Koning T, Sarmiento J, Boric MP, Birukov K, Cancino J, Varas-Godoy M, Soza A, Alves NG, et al. TNF-alpha-activated eNOS signaling increases leukocyte adhesion through the S-nitrosylation pathway. *Am J Physiol Heart Circ Physiol*. 2021;321:H1083–H1095. doi: 10.1152/ajpheart.00065.2021
94. Behmoaras J, Gil J. Similarities and interplay between senescent cells and macrophages. *J Cell Biol*. 2021;220:e202010162. doi: 10.1083/jcb.202010162
95. Walter W, Sanchez-Cabo F, Ricote M. GOplot: an R package for visually combining expression data with functional analysis. *Bioinformatics*. 2015;31:2912–2914. doi: 10.1093/bioinformatics/btv300